Alternative Splicing in TRPA1 Drives Sensory Adaptation to Electrophiles in Drosophilids

Hiromu C. Suzuki,[1,*] Claire T. Saito,[2,3] Srivarsha Rajshekar,[4] Takaaki Sokabe,[3,5,6] Diler Haji,[1] Simon C. Groen,[7,8] Julianne N. Peláez,[1] Teruyuki Matsunaga,[1] Ashleigh S. Takemoto,[1] Kentaro M. Tanaka,[9] Aya Takahashi,[9,10] Makoto Tominaga,[11] Shigeru Saito,[2,3,*] and Noah K. Whiteman[1,4,*]

[1]Department of Integrative Biology, University of California, Berkeley, Berkeley, CA 94720, USA

[2]Graduate School of Biosciences, Nagahama Institute of Bio-Science and Technology, Nagahama 526-0829, Japan

[3]Thermal Biology Group, Exploratory Research Center on Life and Living Systems, National Institutes of Natural Sciences, Okazaki 444-8787, Japan

[4]Department of Molecular and Cellular Biology, University of California, Berkeley, Berkeley, CA 94720, USA

[5]Section of Sensory Physiology, Center for Genetic Analysis of Behavior, National Institute for Physiological Sciences, National Institutes of Natural Sciences, Okazaki 444-8787, Japan

[6]Department of Physiological Sciences, SOKENDAI, Okazaki 444-8787, Japan

[7]Department of Nematology and Department of Botany & Plant Sciences, University of California, Riverside, Riverside, CA 92521, USA

[8]Center for Infectious Disease and Vector Research, Institute for Integrative Genome Biology, University of California, Riverside, Riverside, CA 92521, USA

[9]Department of Biological Sciences, Tokyo Metropolitan University, Hachioji 192-0397, Japan

[10]Research Center for Genomics and Bioinformatics, Tokyo Metropolitan University, Hachioji 192-0397, Japan

[11]Thermal Biology Research Group, Nagoya Advanced Research and Development Center, Nagoya City University, Nagoya 467-8601, Japan

* Correspondence: hiromus@berkeley.edu (H.C.S.), s_saito@nagahama-i-bio.ac.jp (S.S.), whiteman@berkeley.edu (N.K.W.)

ABSTRACT

Behaviors are among the first traits to evolve as animals enter new niches, but their molecular bases are poorly understood. To address this gap, we used the mustard-feeding drosophilid fly *Scaptomyza flava*, which feeds on toxic Brassicales plants like wasabi that produce noxious, electrophilic isothiocyanates (ITCs or mustard oils). We found that *S. flava* exhibits dramatically reduced behavioral sensitivity to allyl isothiocyanate (AITC) compared to its microbe-feeding relatives *S. pallida* and *Drosophila melanogaster*. We hypothesized that molecular evolution of the "wasabi receptor" TRPA1, known to perceive ITCs in flies, could explain this loss of aversion. Our experiments revealed three interconnected evolutionary genetic changes consistent with this hypothesis. First, TRPA1 was expressed in labellar tissues of *S. flava* at the lowest levels among the three species, at a nearly four-fold lower level than in *D. melanogaster*. Second, *S. flava* expressed a higher proportion of TRPA1 splice variants previously reported to be less sensitive to chemical stimulus. Third, we identified amino acid substitutions in *S. flava* that could influence the structure of intracellular domains of TRPA1. To test the functional salience of these mechanisms *in vitro* and *in vivo*, we validated TRPA1 splicing isoforms using *Xenopus* oocyte electrophysiology and the *GAL4/UAS* system in *D. melanogaster*. Single isoform electrophysiology indeed revealed evolution of TRPA1 in the *S. flava* lineage towards reduced electrophile sensitivity. Ectopic expression of *S. flava* TRPA1 in *D. melanogaster* consistently conferred weaker AITC sensitivity *in vivo* than expression of its orthologues, although this did not fully recapitulate differences in wild-type phenotypes between the species suggesting other molecular evolutionary mechanisms were involved. Finally, we explored the consequences of isoform co-expression using oocyte electrophysiology. We found that enrichment of electrophile-insensitive TRPA1 splicing isoforms as observed in *S. flava* can additively reduce cellular responses to AITC, which could further contribute to reduced electrophile aversion. Our findings illuminate how expression differences, protein structural changes, and especially alternative splicing, together can drive sensory evolution as animals behaviorally adapt to toxic new niches.

INTRODUCTION

Animal behaviors are often encoded by complex genetic architectures. This mechanistic complexity has hampered efforts to link variation in genotype with variation in behavior (Bendesky and Bargmann 2011). An exception is the progress being made in understanding how genetic changes in chemosensory genes expressed in the peripheral nervous systems of animals affect behavior. Because of the relative simplicity and modularity of chemosensory functional units, chemosensation offers an appealing window for studying the molecular mechanisms underlying the evolution of behavior (Montell 2021; Valencia-Montoya et al. 2024).

Insects are particularly useful models for addressing these questions because of their experimental tractability and an umwelt rich in volatiles and tastants. The vinegar fly family Drosophilidae, which includes the “fruit fly” *Drosophila melanogaster* and thousands of other species with diverse dietary niches, has played a central role in advancing our understanding of how animal behavior evolves through changes in chemosensation. Fueled by a wealth of genomic resources, genetic tools, and neuroanatomical insight, comparative analyses between *D. melanogaste*r and ecological specialists, such as noni-feeding *D. sechellia* (McBride 2007; McBride and Arguello 2007; Prieto-Godino et al. 2017; Auer et al. 2020; Álvarez-Ocaña et al. 2023), screw pine-feeding *D. erecta* (McBride and Arguello 2007), ripe fruit feeding *D. suzukii* (Karageorgi et al. 2017; Dweck et al. 2021; Wang et al. 2022), and cactus rot-feeding *D. mojavensis* (Diaz et al. 2018; Khallaf et al. 2020), have illuminated evolutionary genetic changes involved in the evolution of new chemosensory-driven behaviors. However, there remains a disconnect between our understanding of the specific molecular changes that give rise to these new behaviors, with few exceptions (Prieto-Godino et al. 2017; Auer et al. 2020).

The fly genus *Scaptomyza*, an ecologically diverse group of 273 species nested within the Hawaiian *Drosophila* clade and sister to the subgenus *Drosophila* clade, provides another promising lineage to investigate this problem. Of particular interest is the subgenus *Scaptomyza*, which includes a number of obligate herbivorous species, such as *Scaptomyza flava*, which attacks many mustard species in the Brassicaceae and relatives in the Brassicales (Whiteman et al. 2011). Unlike their generalist relatives in the other subgenera of *Scaptomyza* that feed on microbes within decaying plant tissues, *S. flava* larvae are leafminers consuming internal cell layers (Aguilar et al. 2024) and adult females use their leaf-cutting ovipositor to create punctures and drink the exudates that seep into the wound (Whiteman et al. 2011; Peláez et al. 2022). Brassicales leaves are defended by both constitutive and inducible specialized metabolites, which impose a unique selective pressure on *S. flava* not imposed by microbial diets (Whiteman et al. 2011; Aguilar et al. 2024).

S. flava was originally reported as a leafminer of mustards in a 1902 report on *Arabidopsis thaliana* from the United States and can be maintained in the laboratory on this species, which allows for experimental manipulation of the host plant using an abundance of available genetic tools (Whiteman et al. 2011). Herbivory evolved in the *Scaptomyza* lineage ca. 10-15 million years ago (Fig. 1A; Lapoint et al. 2013; Matsunaga et al. 2022; Peláez et al. 2022). This relatively recent dietary transition from saprophagy/microbivory to herbivory provides a useful context for identifying the evolutionary genetic changes accompanying this niche shift using a comparative approach. It is also an appealing model for studying the molecular basis of chemosensory evolution. Several host plant-related evolutionary changes in the chemosensory system of *S. flava* have been reported, including the lack of attraction to yeast odors and the gain of attraction to mustard-derived odorants, mediated by gene losses or duplications of respective olfactory receptor (*Or*) genes (Goldman-Huertas et al. 2015; Matsunaga et al. 2022).

The major chemical defense system of mustard plants and their relatives in the Brassicales is known as the "mustard oil bomb." During tissue damage, electrophilic, pain-causing toxins called isothiocyanates (ITCs), commonly known as mustard oils, can be formed through the hydrolysis of non-toxic β-thioglucoside N-hydroxysulfates called glucosinolates (GLSs). Specifically, when plant tissues are mechanically damaged by herbivores, GLSs are hydrolyzed by an enzyme called myrosinase and a subset of the GLS molecules are converted into ITCs, which are highly toxic owing to their electrophilicity and induce robust escaping behaviors in generalist insects, including the fruit fly *D. melanogaster* (Lichtenstein et al. 1964; Kang et al. 2010). Acquisition of this chemical defense system conferred protection against herbivores and is correlated with the diversification of the Brassicaceae ca. 60 million years ago (Edger et al. 2015). A coevolutionary arms race has further shaped counter-defense systems against ITCs on the herbivore side. For example, a lineage of mustard-specializing butterflies, including the cabbage white (*Pieris rapae*), can suppress ITC formation by the action of gut-expressed proteins called nitrile specifier proteins (NSPs), which divert GLS hydrolysis towards non-toxic nitriles, allowing the butterflies to thrive on mustards (Wittstock et al. 2004; Wheat et al. 2007; Okamura et al. 2022). By contrast, *S. flava* allows ITCs to form during herbivory and mitigates mustard oil toxicity using the ancient mercapturic acid pathway (Gloss et al. 2014), which evolved adaptively under pressure from ITCs in *S. flava* (Gloss et al. 2019), but is less efficient at detoxifying GLS-derived defenses than NSPs. Moreover, *S. flava* larvae develop more rapidly when reared on *A. thaliana* loss of function mutants that do not make GLSs required for the production of mustard oils (Whiteman et al. 2012). Thus, *S. flava* encounters ITCs when attacking mustards as adults and developing within them as immatures. Therefore, suppression of behavioral aversion against mustard oils is important for *S. flava* to successfully colonize the leaves of living mustard plants.

A candidate gene that may contribute to this behavioral change in *S. flava* is *TrpA1*, a member of the *Trp* (*Transient receptor potential*) channel gene family. TRPA1 is a well-characterized polymodal cation channel, known as the “wasabi receptor”, that can be activated by various sensory stimuli, including heat, UV radiation, reactive oxygen species, and algogens such as ITCs (Jordt et al. 2004; Talavera et al. 2020; Valencia-Montoya et al. 2024). Like most TRPA1 agonists, ITCs are electrophiles that form covalent bonds with several cysteine residues in the cytoplasmic domain of TRPA1, thereby changing the conformation of the entire channel (Hinman et al. 2006; Macpherson et al. 2007; Zhao et al. 2020). This mechanism-of-action is conserved from vertebrates to flies and planarians (Kang et al. 2010; Arenas et al. 2017). In adult *D. melanogaster*, TRPA1 channels serve a chemosensory function in bitter-sensing (*Gr66a*-expressing) gustatory neurons of the mouthparts (labellum and pharynx) and the legs (tarsi), triggering feeding aversion upon activation (Kang et al. 2010; Leung et al. 2020). Genetic knockout of *TrpA1* disrupts aversion to electrophiles, implying that the TRPA1 channel is the primary gustatory sensor for drosophilids to detect dietary electrophiles (Kang et al. 2010). These observations suggest that the reduced gustatory aversion to ITCs in *Scaptomyza* flies could potentially have evolved through molecular evolution of the TRPA1 channel.

Despite its deep conservation over evolutionary time, there are several cases wherein TRP channels are tied to dramatic sensory adaptations in other animals. For example, a subspecies of the African mole-rat (*Cryptomys hottentotus pretoriae*) is entirely insensitive to allyl isothiocyanate (AITC, the primary ITC in wasabi), possibly as an adaptation that allows tolerance of ant-derived acidic toxins that the mole-rats encounter in their subterranean burrows (Eigenbrod et al. 2019). The lack of pain sensation in this species is correlated with a reduced chemical sensitivity of TRPA1 due to the substitution of one of the key cysteine residues, providing a simple molecular mechanism for the behavioral change (Eigenbrod et al. 2019). Variation in heat activation thresholds of TRPA1 were also observed among reptiles and amphibians in relation to species-specific thermal niches (Gracheva et al. 2010; Cordero-Morales et al. 2011; Akashi et al. 2018; Saito et al. 2022), suggesting that modification of the channel’s response properties might be a common strategy underlying ecological adaptation. A more complex example is found for another vertebrate heat sensor, TRPV1, in the vampire bat (*Desmodus rotundus*). This blood-feeder senses infrared signals from mammalian prey using pit organs. In a comparison with non-infrared-sensing bat species, TRPV1 of the vampire bat encoded two splicing isoforms with different threshold temperatures and this bat’s trigeminal neurons were highly enriched for a isoform with a truncated C-terminus that activates at a lower temperature than the a canonical isoform. The skewed expression ratio in favor of the splice isoform with higher heat sensitivity likely allows the vampire bat to sense the slightly elevated temperature in its prey that emit infrared (Gracheva et al. 2011).

Given these findings, we hypothesized that the *TrpA1* gene has also experienced adaptive evolution in the genus *Scaptomyza* owing to the novel chemical environment provided by the mustard host plants of *S. flava*, which produce ITCs upon tissue damage. Specifically, we addressed the working hypothesis that molecular evolution of TRPA1 facilitated specialization onto mustard host plants in the *S. flava* lineage by weakening gustatory aversion to ITCs. To this end, we conducted a behavioral screen followed by an in depth investigation of the characteristics of TRPA1 across three drosophilid species from different phylogenetic placements and with different diets: the mustard specialist herbivore *S. flava*, the closely related generalist microbivore *S. pallida*, and the rotting fruit and yeast-feeding *D. melanogaster*. Between the three focal species, we compared gene-level and splicing isoform-level expression profiles of the *TrpA1* gene and physiological responses of TRPA1 channel splicing isoforms against electrophiles. Our results indicate that reduced channel activity through protein evolution and modulation of alternative splicing in TRPA1 are indeed two key mechanisms correlated with adaptation to a specialized diet of mustard plants in *S. flava*. We conclude that incremental changes in multiple molecular mechanisms together can give rise to behavioral novelties.

RESULTS

Gustatory aversion of isothiocyanates is attenuated in *S. flava*.

We first characterized feeding inhibition of flies in response to dietary AITC by monitoring PER (proboscis extension reflex) to tarsal/labellar stimulation (Shiraiwa and Carlson 2007; Kang et al. 2010). After a 24-hour starvation period, flies were challenged with a single concentration of AITC mixed in sucrose solution as test stimulus. Responses of individual flies were scored as a proxy of feeding inhibition by AITC and normalized to responses towards a control stimulus of 0 mM AITC in a range between 0 and 1, wherein a smaller score indicated stronger aversion (See Methods for details). This feeding assay showed that the two microbe-feeding species, *D. melanogaster* and *S. pallida*, clearly exhibited a stepwise reduction in feeding responses of female flies as the AITC concentration increased (Figure 1B). By contrast, females of the mustard specialist *S. flava* did not show a significant feeding aversion towards AITC throughout the gradient, although we observed a slight reduction of PER at 10 mM AITC (approx. 13% lower than the 0 mM AITC; Figure 1B). This attenuated aversion towards AITC was also observed in male *S. flava* (Figure S1), despite the fact that they do not feed on plant exudates because they cannot pierce leaves, at least under laboratory conditions (Peláez et al. 2022). This suggests that while the behavioral aversion towards AITC in *S. flava* is not entirely lost, it is significantly weakened compared with its microbe-feeding relatives, consistent with our working hypothesis.

Given that food-associated odorants can promote feeding in *D. melanogaster* (Shiraiwa 2008; Oh et al. 2021), we also addressed whether and to what extent volatile ITCs from plants could enhance feeding in *S. flava*, which would mitigate contact-mediated ITC aversion and might then explain the PER assay results. We repeated the PER assay in *S. flava* after surgically removing the antennae and maxillary palps to disrupt its olfactory inputs (Figure S1). We found that *S. flava* flies did not exhibit any significant increase or decrease of feeding rates based on AITC concentrations (Figure S1), in contrast to the slight aversion towards AITC observed in intact male flies (Figure S1). This pattern suggests that volatile ITCs – at least AITC – do not enhance feeding in *S. flava*.

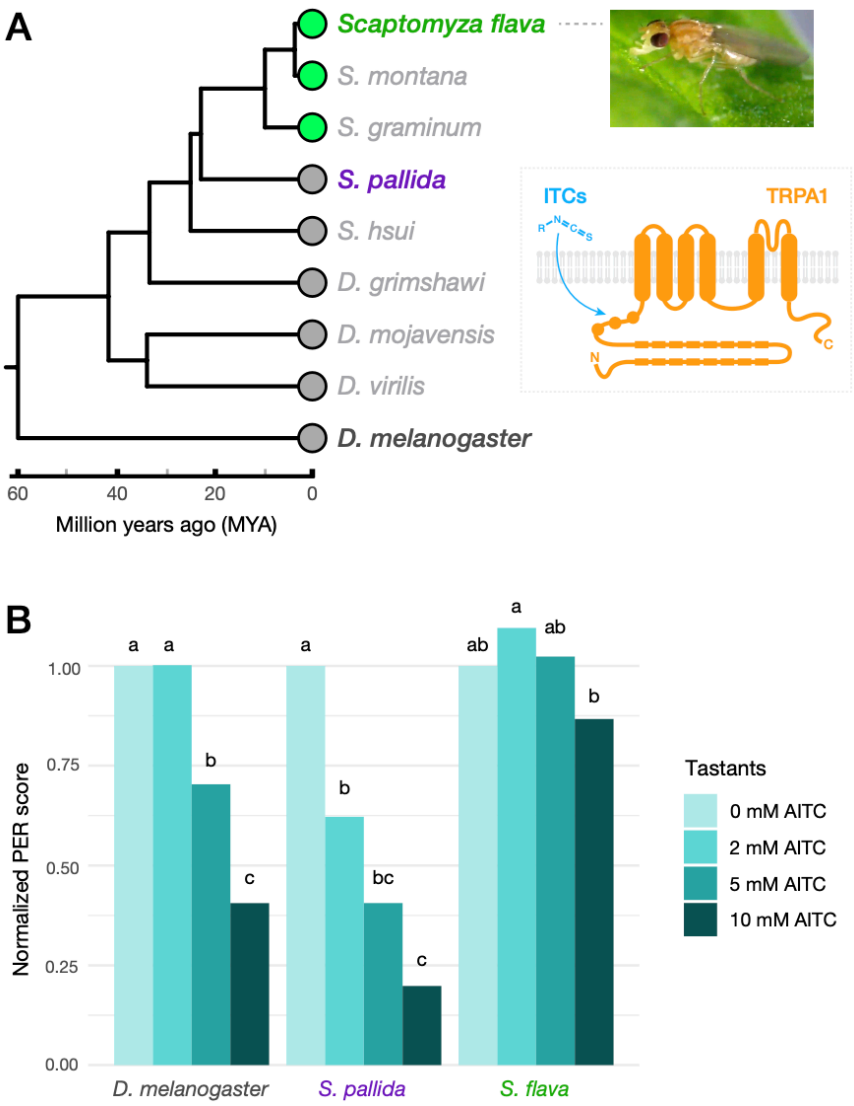

Figure 1. *Scaptomyza flava* exhibits attenuated feeding aversion against allyl isothiocyanate (AITC). (A) (Left) A time-calibrated species tree of drosophilids, including the genus *Scaptomyza*, based on 11 nuclear and mitochondrial genes (Matsunaga et al. 2022; Peláez et al. 2023). Colored circles at the tree tip represent the feeding ecology of the species (Grey: Microbivory, Green: Obligate herbivory). (Right) *Scaptomyza flava* female and a diagram of a TRPA1 channel targetted by isothiocyanates (ITCs). (B) Results of PER assay using adult females of the three focal species (*D. melanogaster*, *S. pallida*, and *S. flava*) at four different concentrations of AITC mixed in 300 mM sucrose solution. PER score of a single fly represents the feeding response to a given tastant over five trials. Bars indicate average PER scores for each treatment (n = 19-34 per treatment), normalized to the score at 0 mM AITC within each species. Letters indicate significant differences between tastants within species based on pairwise Wilcoxon rank-sum test with Benjamini-Hochberg correction ($p < 0.05$).

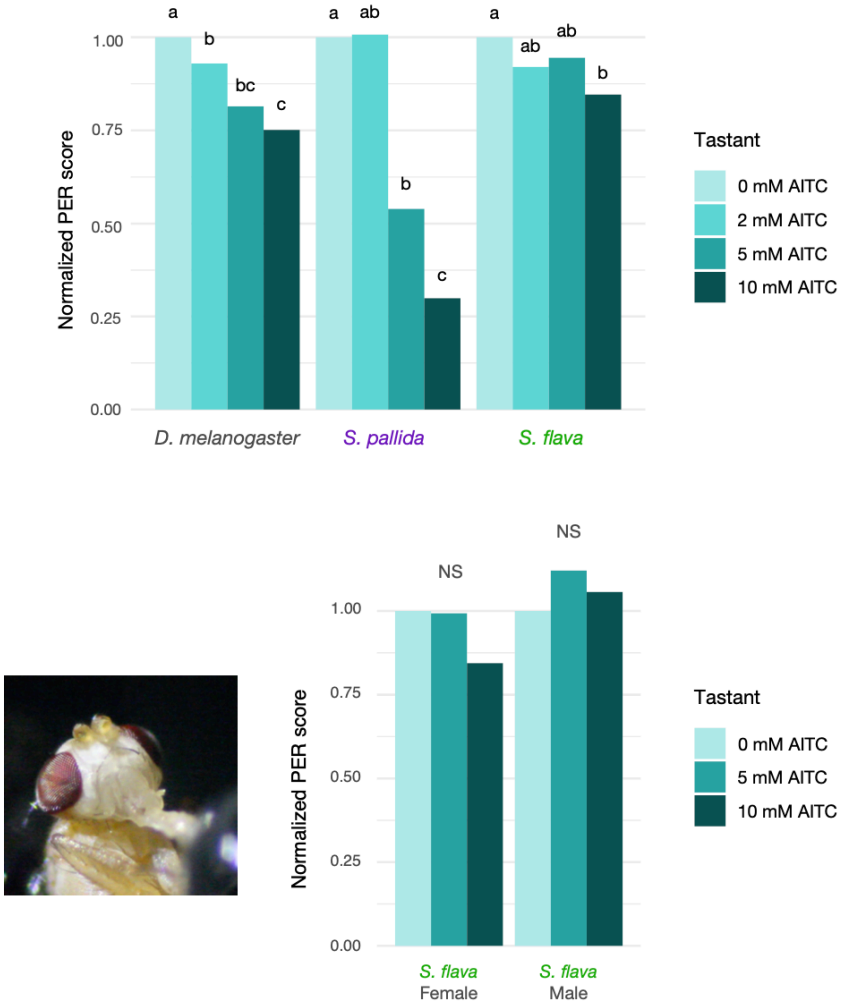

Supplementary Figure S1. Additional data of PER assay. (Top) Results of PER assay using male flies from the three focal species (n = 20-32 per treatment). (Bottom left) A photograph of *S. flava* female with their antennal segments (3rd and 4th) and maxillary palps removed. (Bottom Right) Results of PER assay in antenna/palp-less *S. flava* (n = 9-14 per treatment). For both PER assays, average PER scores were normalized to that of 0 mM AITC. Differences in PER scores between tastants within species or sexes were analyzed by pairwise Wilcoxon rank-sum test with Benjamini-Hochberg correction ($p < 0.05$).

Another hypothesis for these behavioral differences is that *S. flava* was hungrier than the other species after the starvation period prior to the assay, such that bitter sensation at the periphery was overridden by strong appetite (Inagaki et al. 2014; Yapici et al. 2016). To explore this possibility, we ran a simple hunger tolerance assay to monitor the survival rate of flies in foodless, humidified vials (Li et al. 2016). We found that hunger tolerance significantly varied between the species (Figure S2), and that the survival rates of *S. flava* were intermediate between those of *D. melanogaster* and *S. pallida* (Figure S2). In both sexes, *D. melanogaster* was most susceptible to the starvation treatment. *S. flava* and *S. pallida* were comparable in hunger tolerance up to 100-150 hours, but afterwards, *S. pallida* exceeded the tolerance of *S. flava* (Figure S2). The fact that the aversion towards AITC was clearly observed in the species at the two extremes of hunger tolerance (i.e., *D. melanogaster* and *S. pallida*), but not in *S. flava*, indicates that hunger does not explain the variation in AITC aversion across species. Taken together, we conclude that the weak aversion towards AITC in *S. flava* could be attributed to lineage-specific modifications of the sensory system, most likely in their gustatory neurons given that these neurons are responsible for mediating AITC detection through TRPA1.

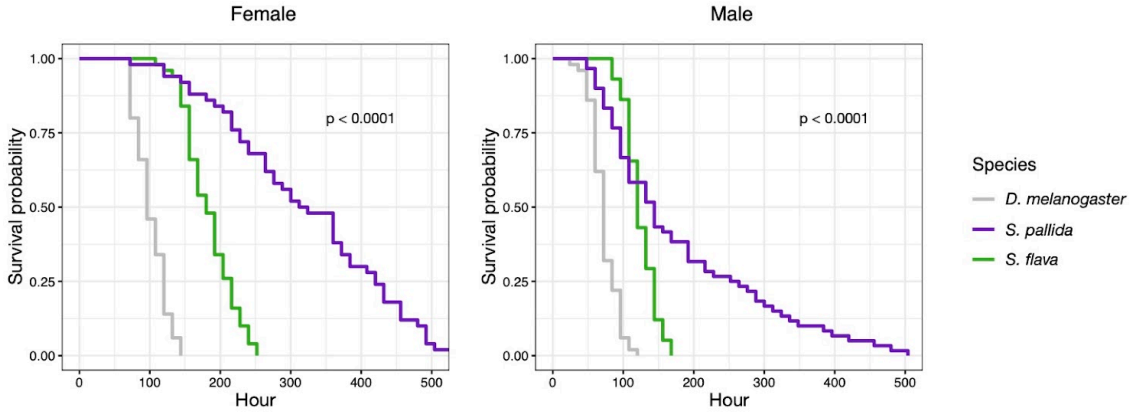

Supplementary Figure S2. Hunger tolerance assay of adult flies. Survival plots of (Left) female and (Right) male flies, each of which consists of n = 5-6 independent groups of 8-10 flies. Differences between species were analyzed by log-rank test. Only group-wide *p*-values were shown.

Cross-species variation in *TrpA1* gene expression.

The *TrpA1* gene is intact in the *S. flava* genome and encodes an open reading frame. Bulk tissue RNA-sequencing confirmed robust expression of *TrpA1* in labella and tarsi of both *S. flava* sexes (Figures 2A-2F; Figure S3). Cross-species DEG analyses identified *TrpA1* as a differentially expressed gene in all comparisons but with varying degrees. For example, labellar *TrpA1* expression in *S. pallida* was only slightly higher than that in *S. flava* (Figures 2A and 2C), whereas there was almost four-fold higher expression in *D. melanogaster* compared to *S. flava* (Figures 2B and 2C). The ranks of *TrpA1* expression levels were reversed in tarsi, where *S. flava* showed the highest expression (Figures 2D-2F). This leg transcriptome analysis should be interpreted cautiously, however, because the *D. melanogaster* expression data were derived from both tarsi and tibia (Wang et al. 2022), while our *Scaptomyza* expression data were derived from tarsal segments alone. Nonetheless, these transcriptome patterns highlighted cross-species variation in *TrpA1* expression levels that could influence the differences in gustatory behaviors we observed.

Changes in chemosensory preferences could also be induced by receptor misexpression among sensory neurons. To characterize the types of neurons expressing TRPA1 channels, we visualized mRNA localization in the labellum of *S. flava* and *D. melanogaster* using HCR (hybridization chain reaction) RNA-FISH (Choi et al. 2018). We found in *S. flava* that signals of *TrpA1* mRNA formed neuron-like clusters and always co-localized with those of *Gr66a*, a marker of bitter-sensing gustatory neurons (Figure 2J-2L). This pattern was also consistent with our HCR images of *D. melanogaster* labella (Figure 2G-2I), as well as those from a previous study (Leung et al. 2020). These results showed that *TrpA1* expression in bitter-sensing gustatory neurons are conserved between the two lineages, indicating *S. flava* still perceives ITCs as deterrents despite their mustard-feeding ecology.

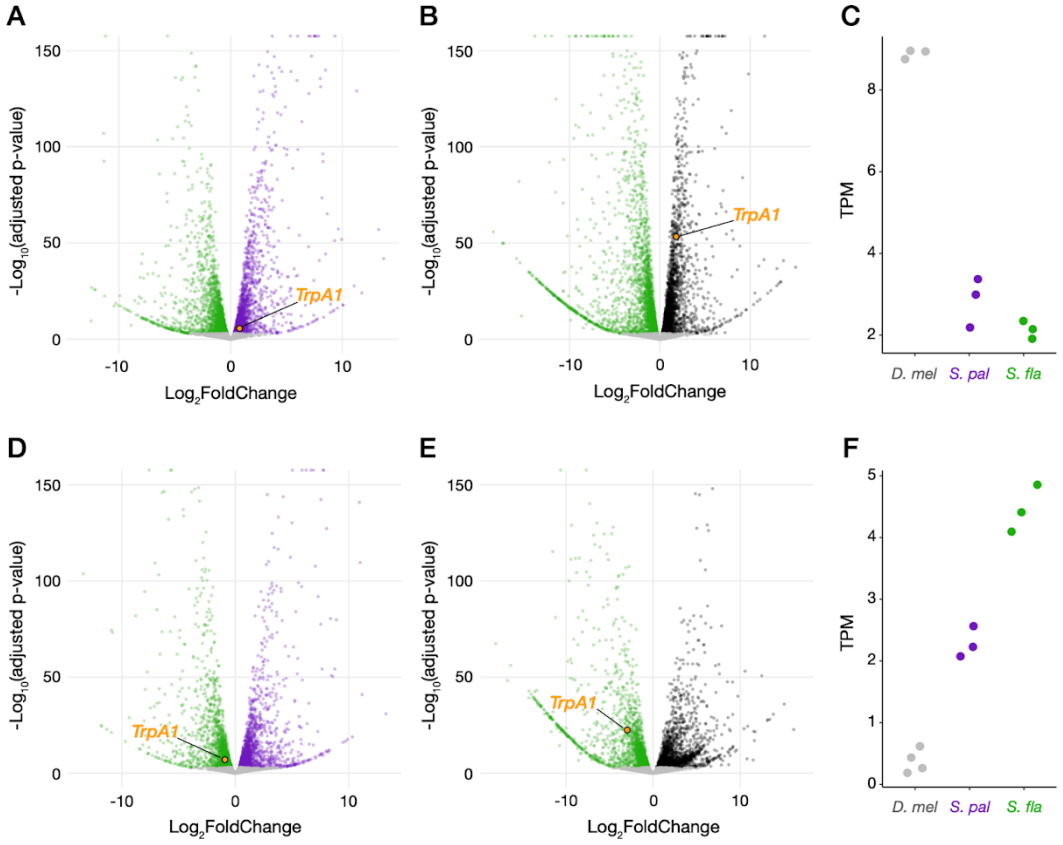

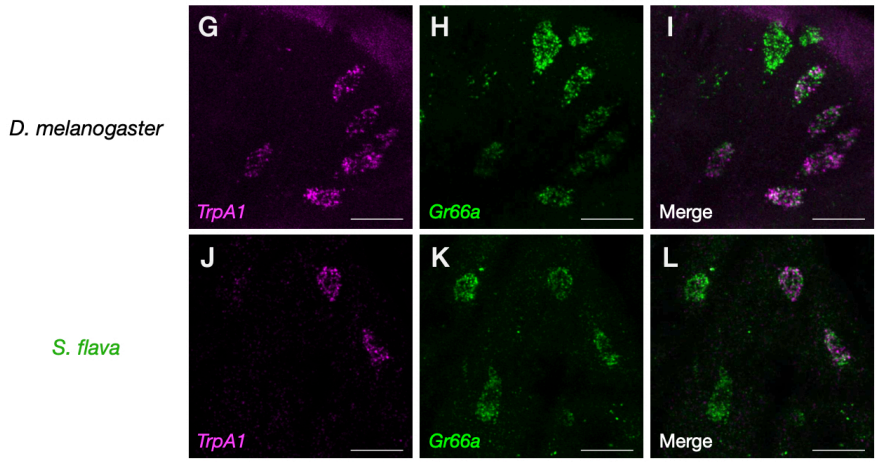

Figure 2. Gene expression of *TrpA1* is quantitatively variable but spatially conserved across drosophilids. (A, B) Volcano plots of cross-species DEG analysis using female labellar (mouth) transcriptome between (A) *S. flava* - *S. pallida*, and (B) *S. flava* - *D. melanogaster*. Colored dots represent differentially expressed genes between species (adjusted *p*-value < 0.001). (C) TPM (transcripts per million) values from labellar transcriptomes (n = 3 per species). (D, E) Volcano plots of cross-species DEG analysis using female tarsal (leg) transcriptome between (D) *S. flava* - *S. pallida*, and (E) *S. flava* - *D. melanogaster*. Colored dots represent differentially expressed genes between species (adjusted *p*-value < 0.001). (F) TPM values from tarsal transcriptome (n = 3-4). Note that *D. melanogaster* transcriptome data used here were obtained from (Dweck et al. 2021) and (Wang et al. 2022). (G-L) Confocal images of labella from (G-I) *D. melanogaster* female and (J-L) *S. flava* female, showing fluorescent signals from *TrpA1* (magenta; G, J), *Gr66a* (green; H, K), and merged mRNAs (I, L). Scale bars represent 10 μm.

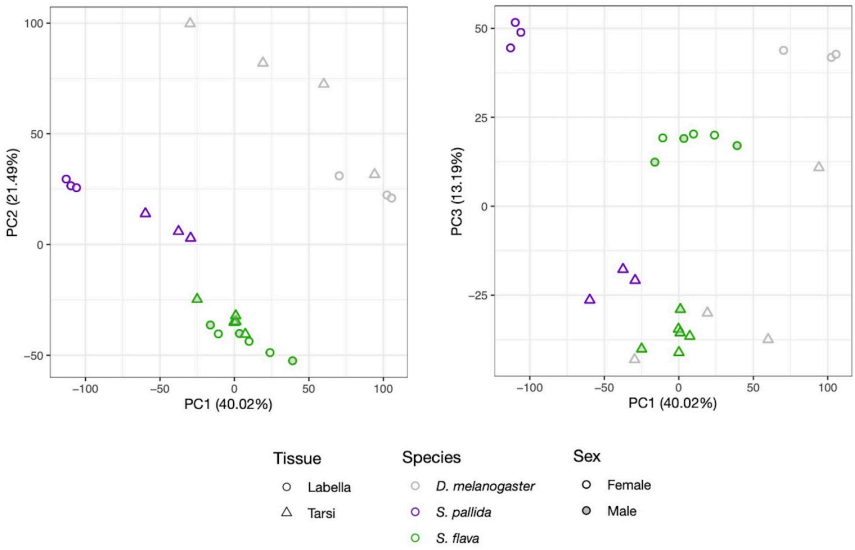

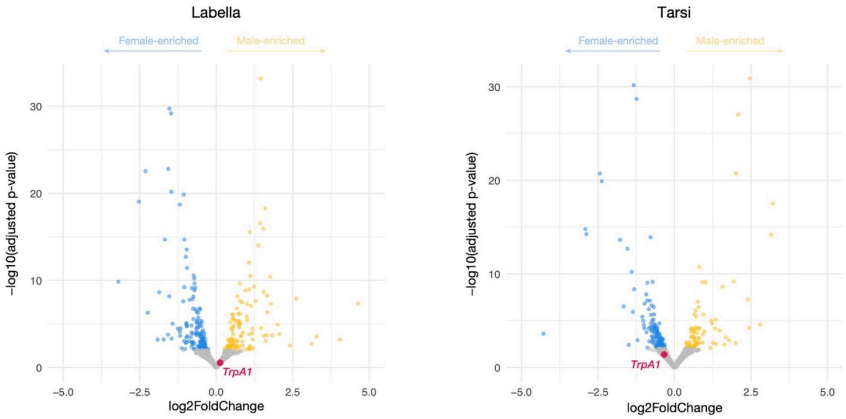

Supplementary Figure S3. Labellar and tarsal transcriptome analyses. (Top) PCA plots for 25 transcriptome datasets based on read count data of 8,920 orthologous genes. (Bottom) Volcano plots of DEG analysis between female and male *S. flava*. *TrpA1* was not differentially expressed between sexes in both labella and tarsi.

Compositions of *TrpA1* splicing isoforms vary predictably across species.

The *D. melanogaster TrpA1* gene undergoes alternative splicing to produce five isoforms with variable expression and functional properties (Kang et al. 2012; Zhong et al. 2012; Gu et al. 2019; Leung et al. 2020; Gu et al. 2022; Sato et al. 2023; Du et al. 2024). These differences in TRPA1 splicing isoform function could potentially also be exploited during adaptation to dietary electrophiles as a source of sensory innovation in *S. flava* as in the case of the truncated TRPV1 splicing isoform that evolved in infrared-sensing vampire bats (Gracheva et al. 2011).

To this end, we investigated the structures and quantified the compositions of *TrpA1* splicing isoform mRNAs across *Drosophila/Scaptomyza* species and across the salient gustatory organs. Initial *de novo* assembly of RNA-sequencing reads revealed the presence of at least five *TrpA1* splicing isoforms expressed in the labella/tarsi of *S. flava* and *S. pallida* (Figure 3A). All *Scaptomyza TrpA1* splice variants contained Exons 1 and 2, showing similarities to the *TrpA1-C/D/E* splicing isoforms of *D. melanogaster* (Figure 3A). We found negligible expression of *TrpA1-A/B* analogues in *S. flava* labella and tarsi, and little expression of these in *S. pallida*, although the first exonic sequence (i.e., Exon 3) was intact in both genomes (Figure S4). Intriguingly, all *Scaptomyza* spp. *TrpA1s* acquired two additional exons upstream of Exon 1, named Exon L and Exon S ("Longer" or "Shorter" exons), each of which provided a putative start codon for different splicing isoform types (Figure 3A; Figures S4 and S5). Genomic comparisons revealed that Exon L appeared at least in the common ancestor of the subgenus *Drosophila* and retained some sequence similarity to the 5' UTR of *D. melanogaster TrpA1*, implying a potentially ancient evolutionary origin of this motif (Figures S4 and S6). Exon S likely evolved at the base of the Hawaiian *Drosophila* and *Scaptomyza* clades, although we lacked transcriptional data for most species (Figures S4 and S6). These newly-discovered *Scaptomyza TrpA1* splicing isoforms were named *TrpA1-CL/CS/DL/DS/EL*, respectively, based on the choice of exons and their homology to *D. melanogaster TrpA1* splicing isoforms (Figure 3A; adopting the nomenclature from (Zhong et al. 2012)). The presence of these splicing isoforms was further validated by subcloning and plasmid Sanger sequencing.

Quantification of splicing isoform expression posed a challenge in the case of *Scaptomyza TrpA1*. Because exons that define splicing isoforms are distantly located on mRNAs (i.e., Exons L/S and 12/13 are approximately 2 kb apart; Figure 3A), we could not accurately parse out the expression of each splicing isoform using short-read RNA-sequencing or quantitative PCR. To address this issue, we carried out amplicon sequencing of *TrpA1* transcripts using a MinION long-read sequencer (Oxford Nanopore Technologies) that covers up to 4 Mb in a single read. Briefly, we PCR-amplified the entire repertoire of *TrpA1* transcripts from labellar or tarsal cDNA (except for *TrpA1-A/B*), sequenced them on the MinION, and sorted each sequence read into a closest isoform type using BLAST searching, assuming isoform compositions were

351 maintained throughout the process (Clark et al. 2020; Figure S7). This approach
352 revealed substantial variation in the composition of *TrpA1* splicing isoform expression
353 across species and organs (Figure 3B), except for *D. melanogaster* tarsi, which failed
354 the cDNA recovery due to low *TrpA1* expression levels (Figure 2F). Notably, while the
355 *TrpA1-CL* (*TrpA1-C*) splicing isoform was predominant in *D. melanogaster* and enriched
356 in *S. pallida* labella, *TrpA1-DL* was more represented in *S. flava* labella (Figures 3B and
357 3C). Differences between tissues were also striking, wherein *TrpA1-DL* tended to be
358 more abundant in tarsi than in labella (Figure 3B and 3C). Isoforms containing Exon S,
359 *TrpA1-CS* and *-DS*, were almost exclusively detected in *S. flava,* while the expression of
360 *TrpA1-EL* was only visible in *S. pallida* (Figure 3B; Figure S8). These unique
361 proportions of *TrpA1* splicing isoforms suggest that the differences in splicing isoform
362 compositions might be linked to the behavioral variation across fly species.

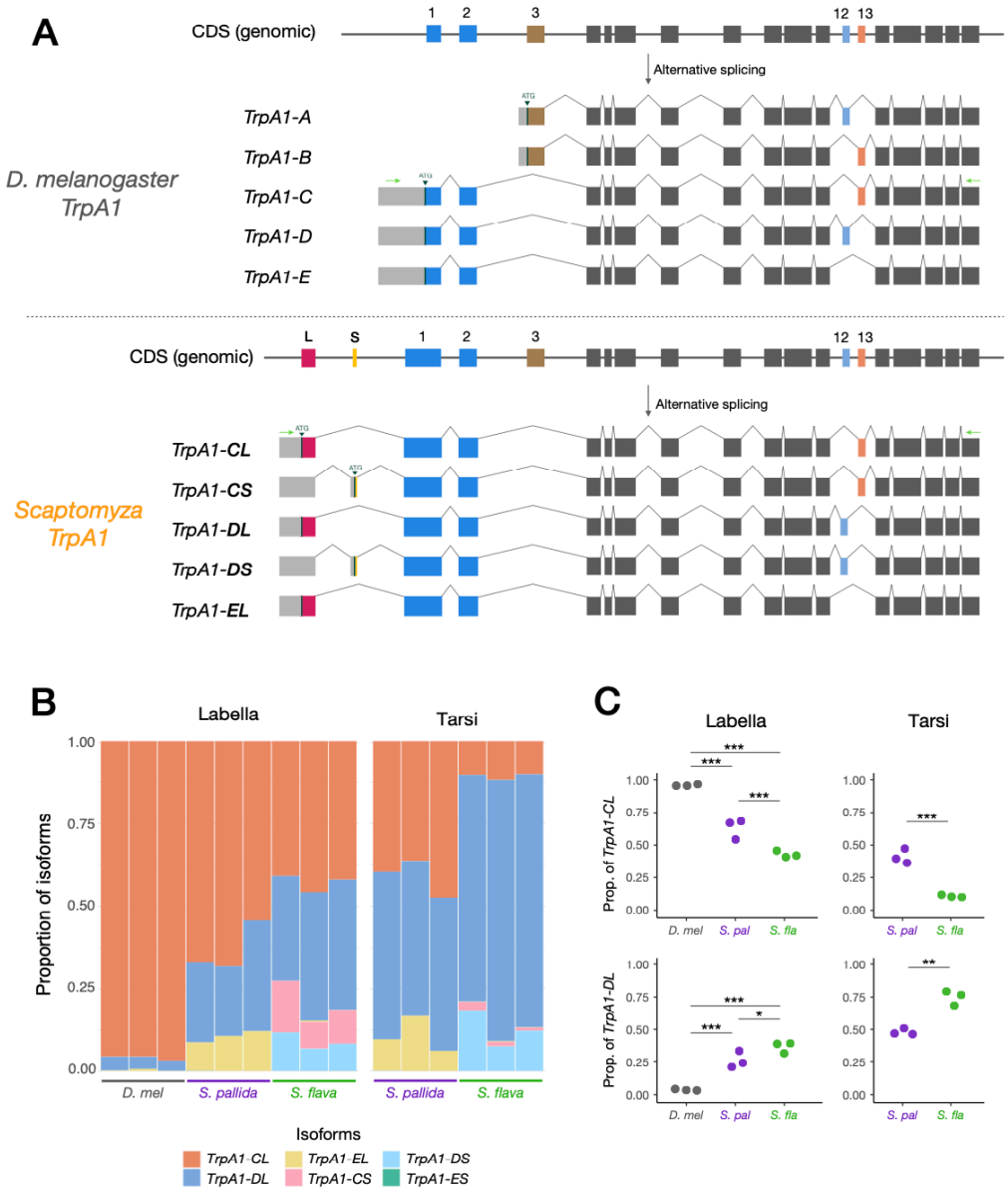

Figure 3. Compositions of *TrpA1* splicing isoforms vary among species. (A) Exon-intron structures of *TrpA1* splicing isoforms of *D. melanogaster* and *Scaptomyza* (i.e., those identified from *S. flava* and *S. pallida*). Small arrowheads indicate putative translation start sites, whose upstream are putative 5'UTR sequences (grey). Green horizontal arrows indicate the positions of PCR primers designed for amplicon sequencing (see Figure S7). (B) Compositions of *TrpA1* isoforms from female labelar and tarsal cDNA of the three focal species. Each vertical bar represents a single cDNA sample derived from an independent set of 40-50 flies. Note that *D. melanogaster TrpA1-C/D/E* splicing isoforms here were categorized as *TrpA1-CL/DL/EL*, respectively, because of the sequence similarity between its 5'UTR region and Exon L of *Scaptomyza TrpA1s* (see also Figures S4 and S6). *TrpA1-ES* was not detected in transcriptomes of any of the species but included as a potentially produced isoform. (C) Relative abundances of *TrpA1-CL* and *-DL* in labellar and tarsal cDNA derived from individual sets of 40-50 flies (n = 3 per species). Variation in splicing isoform compositions among species was modeled by GLM with Gaussian distribution. Labellar compositions were further tested by Tukey's post-hoc test with Benjamini-Hochberg correction. *: $p < 0.05$, **: $p < 0.01$, ***: $p < 0.001$.

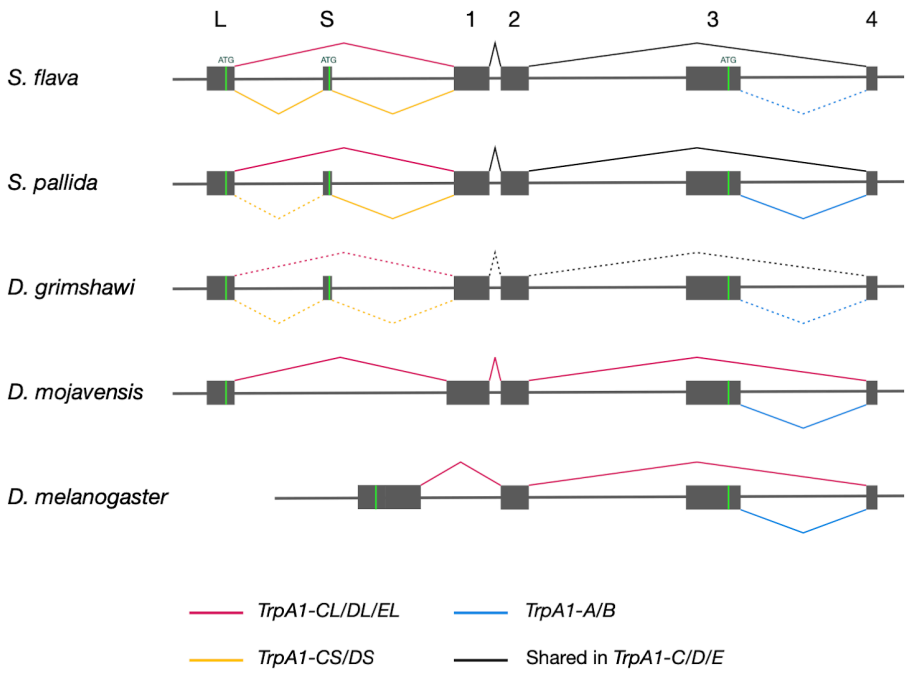

Supplementary Figure S4. Evolution of N-terminal exons of *TrpA1* across drosophilids. Colored lines indicate exon-intron boundaries specific to each isoform type. Dashed lines show the lack of transcriptional evidence (inferred only from genomic/CDS-level information). Green vertical lines indicate putative (i.e., the most upstream) translation start sites for each isoform.

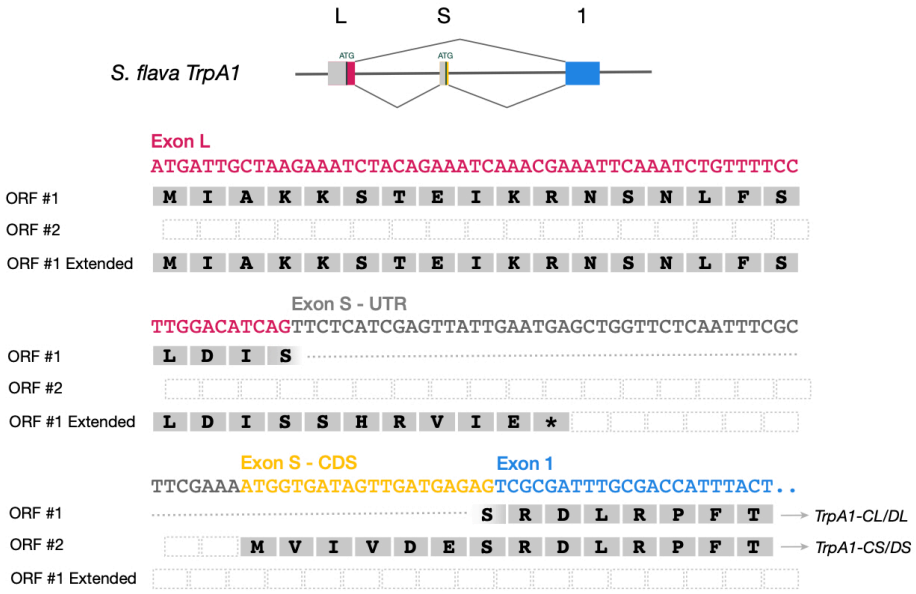

Supplementary Figure S5. Open reading frames (ORFs) of *S. flava TrpA1* splicing isoforms. N-terminal exons and potential ORFs are shown. ORF#1 is likely a splice variant of *TrpA1-CL/DL* splicing isoforms where Exon L directly connects to Exon 1. When Exon S is incorporated into a spliced mRNA, however, ORF#1 would soon encounter a premature stop codon. Longest products would be translated from ORF#2 for *TrpA1-CS/DS* isoforms, which results in shorter products despite the longer mRNAs. The entire Exon L may be a 5'UTR for the translation of *TrpA1-CS/DS* isoforms.

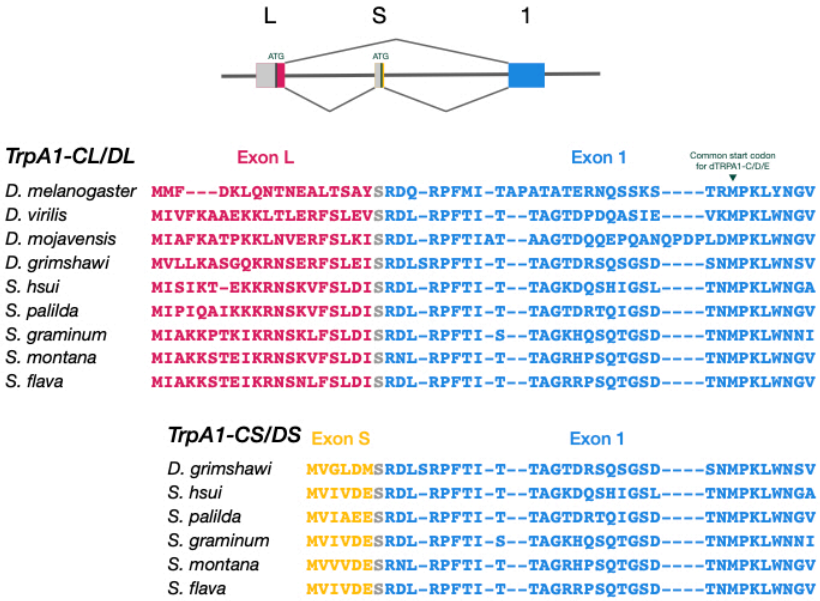

Supplementary Figure S6. N-terminal protein alignments of *TrpA1* splicing isoforms across drosophilids. Note that Exon L and Exon 1 of *D. melanogaster TrpA1* together form a single exon (see Figure S4), the majority of which is usually treated as 5'UTR.

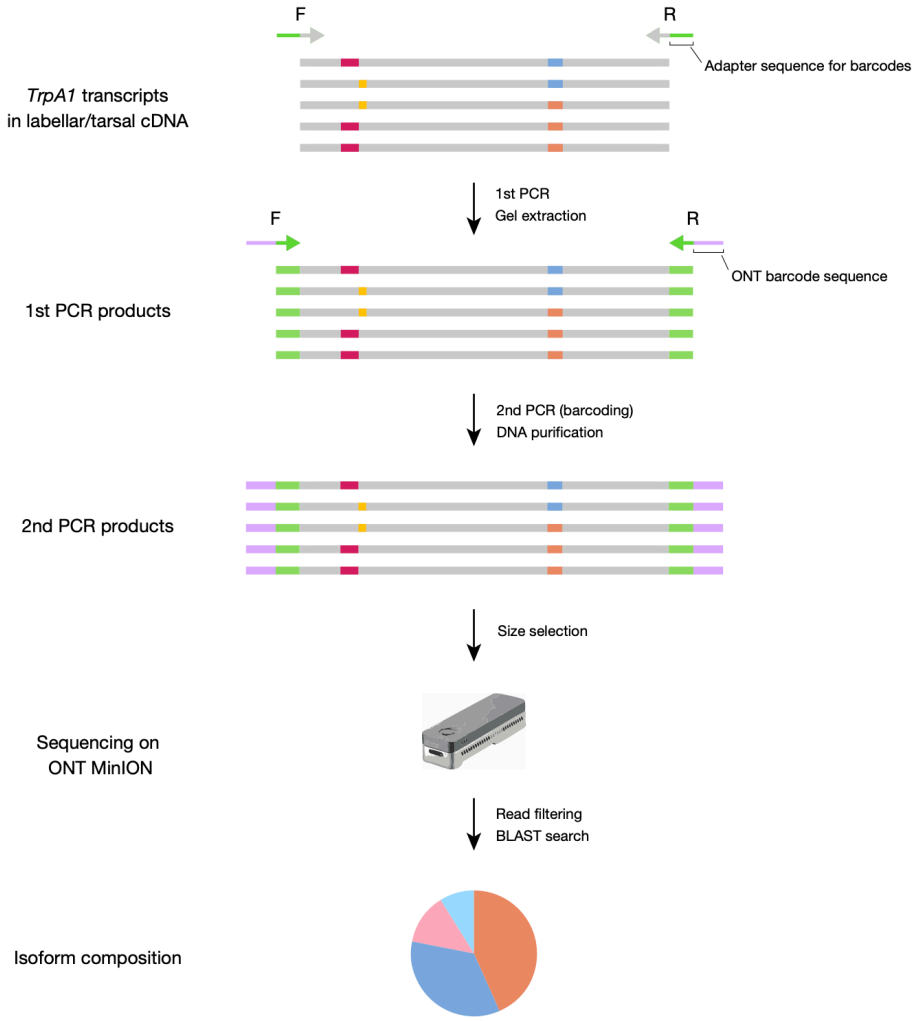

Supplementary Figure S7. A schematic diagram of *TrpA1* amplicon sequencing. Colored regions indicate alternatively spliced exons. An original image for ONT MinION sequencer was obtained from: https://store.nanoporetech.com/us/minion-mk1b-basic-starter-pack.html.

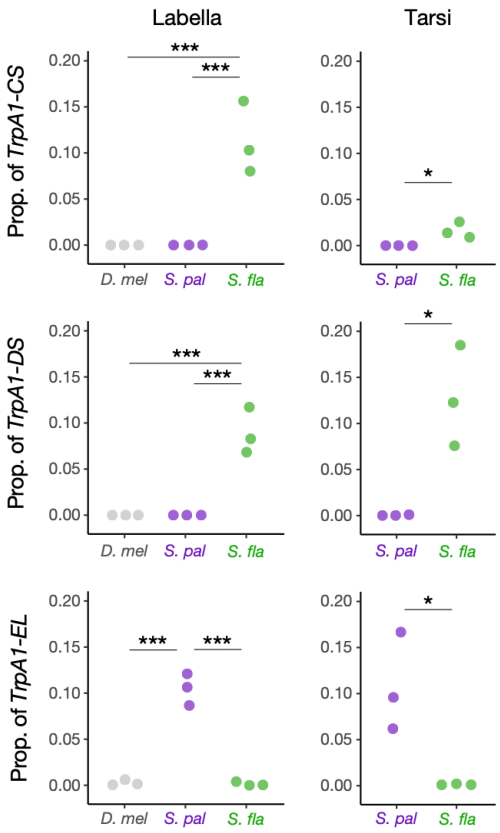

Supplementary Figure S8. Relative abundances of *TrpA1-CL/DL/EL* splicing isoforms. Variation among species (*D. melanogaster* or *D. mel*, *S. pallida* or *S. pal*, and *S. flava* or *S. fla*) was modeled by GLM with Gaussian distribution. Labellar comparisons were further tested by Tukey's post-hoc test with Benjamini-Hochberg correction. *: $p < 0.05$, **: $p < 0.01$, ***: $p < 0.001$.

Herbivore-specific substitutions may modify ankyrin repeat structures of TRPA1

We further searched for potential species-specific amino acid substitutions that could influence the overall structures and physiology of TRPA1 channels. Unlike the case of TRPA1 in the pain-insensitive African mole-rat, cysteine residues required for channel activation (Hinman et al. 2006; Kang et al. 2010) were conserved in all *Drosophila* and *Scaptomyza* TRPA1s investigated (Figure S9), eliminating loss of cysteines as a hypothesis for reduced feeding aversion to electrophiles.

Variation in the number of intracellular ankyrin repeat domains (ARDs) is another potential candidate. ARDs were previously implicated to underlie interspecific variation in thermal and chemical response properties of the TRPA1 channel (Cordero-Morales et al. 2011). We found that amino acid sequences of ARDs were highly conserved in general: only four residues (out of ~600) were uniquely different in *S. flava* and conserved between *S. pallida* and *D. melanogaster*. The four substitutions, Y183F, V244A, D395E, and N501S, corresponded to the 1st, 3rd, 7th, and 10th ankyrin (ANK) domains, respectively (Figure S10). Among these, F183, A244, and E395 were shared within the herbivorous *Scaptomyza* clade, which includes the mustard specialists *S. flava* and *S. montana* as well as a specialist on the pink family (Caryophyllaceae), *S. graminum*. S501 was even more lineage-specific and only identified in *S. flava* and *S. montana*.

To gain insight into the contributions of the herbivore-specific substitutions, we computationally predicted the TRPA1 ARD structures using the AlphaFold Server (Abramson et al. 2024). This analysis raised V244A and N501S as particularly interesting candidate substitutions that could modify hydrogen bonds around the residue (Figure S10). For example, A244 in *S. flava* TRPA1 allowed the formation of a hydrogen bond between R248 and E280, while with V244 this interaction was not formed (Figure S10). Since both alanine and valine have non-polar side chains that do not form hydrogen bonds themselves, this structural difference might be interpreted as the larger side chain of valine potentially preventing the interaction between 248 and 280, while alanine may place the two residues in closer proximity and allow their electrostatic interactions. S501 was predicted to form hydrogen bonds with three adjacent residues (E497, Q498, C502), whereas N501 did not interact with any of these (Figure S10). These predictions suggest that observed herbivore-specific substitutions can change the secondary structures of ARDs via modification of hydrogen bonds, thereby potentially influencing the physiology of TRPA1 channels. Structure-function experiments are needed to more fully address these hypotheses.

Supplementary Figure S9. Key cysteine residues of TRPA1 are conserved across drosophilids. ITCs and many other TRPA1-activating chemicals are known to form covalent bonds with a few intracellular cysteine residues to trigger gating of the channel. Three important cysteines implicated in human TRPA1 (Hinman et al. 2006) are highlighted. Positions of amino acid residues are based on the order of *S. flava* TRPA1. Note that the cysteine at 769th residue falls on Exon 12, which is an alternatively spliced exon and only present in homologues of TRPA1-A/D.

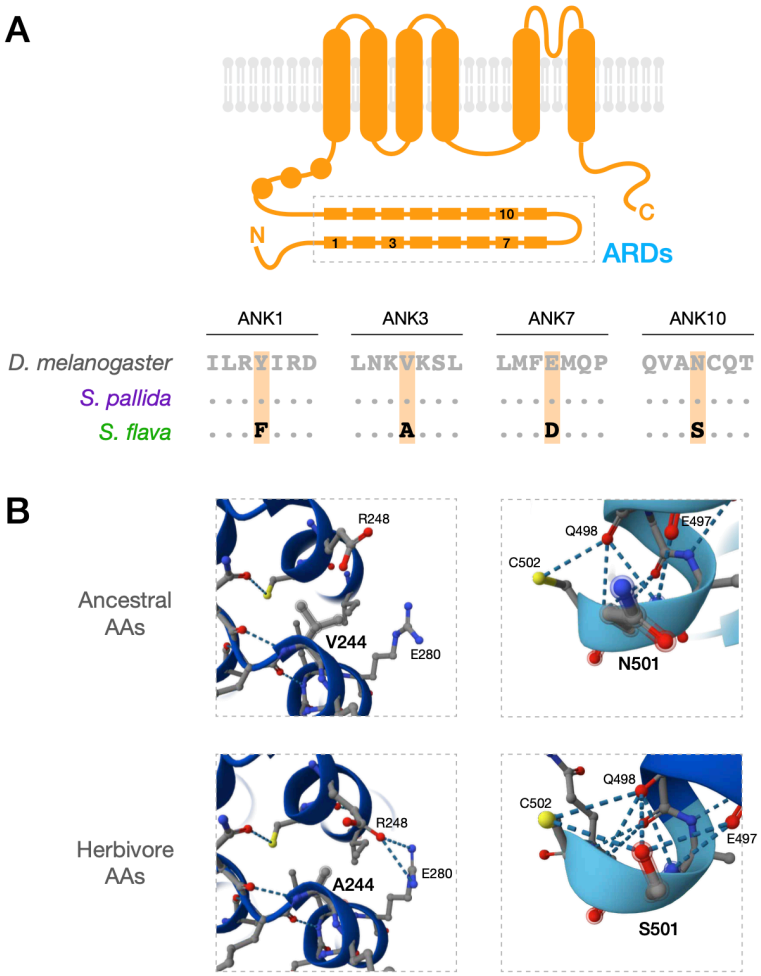

Supplementary Figure S10. Herbivore-specific amino acid substitutions potentially modify the secondary structure of TRPA1. (A) A cartoon of a single TRPA1 protein highlighting the four amino acid substitutions in ankyrin repeat domain (ARD) that were only found in herbivorous species. (B) AlphaFold-led prediction of the secondary structure and hydrogen bonds at 244th (Left, 3rd ANK domain) and 501st (Right, 10th ANK domain) residues of TRPA1 ARD. Dashed lines indicate predicted hydrogen bonds between adjacent residues. The top row shows predictions with ancestral amino acids (V244, N501), while the bottom row shows those with herbivore-specific amino acids (A244, S501).

447 **TRPA1 channels show species-specific responses to AITC *in vitro***

448 We next characterized differences in functionalities of TRPA1 channel splicing isoforms
449 detected from the three drosophilids using two-electrode voltage clamp (TEVC)
450 recordings with *Xenopus laevis* oocytes. As reported previously (Kang et al. 2010), we
451 observed that drosophilid TRPA1 channels stimulated by AITC did not immediately
452 return to the baseline current (Figures 4A-4G), likely due to their unique mode of
453 channel activation (Hinman et al. 2006; Macpherson et al. 2007). This property
454 prevented us from applying a standard current normalization method in which a single
455 cell is consecutively stimulated by multiple dosages such that raw current sizes are
456 corrected by a maximum current amplitude. Instead, we used a strategy in which
457 TRPA1-expressing oocytes were initially stimulated by heat (>40 °C) and subsequently
458 by a single application of AITC, such that an AITC-evoked peak current amplitude (I_{AITC})
459 was normalized by a heat-evoked current (I_{Heat}) at each recording (Figure 4A). This
460 approach assumed that the sizes of heat-evoked currents reflected the degree of
461 TRPA1 expression in oocytes, which was supported by the positive correlations
462 between the two raw current sizes (Figure S11), and succeeded in reducing variances
463 in the raw current data. We repeated measurements across concentration gradients of
464 AITC and eventually predicted a dose-response relationship based on normalized
465 current values (I_{AITC}/I_{Heat}) for each isoform to analyze the physiological property of a
466 channel (Figure 4A). Here, our main interests were the maximum current amplitude,
467 representing the strength of channel activation, and the median effective concentration
468 (EC_{50}), representing the sensitivity of the channel to a chemical stimulus.

469 Under this framework, we conducted cross-species comparisons of AITC
470 dose-responses for TRPA1-CL and TRPA1-DL, the two "canonical" TRPA1 splicing
471 isoforms of *Scaptomyza* (Figure 3B and Figure S6; again, we considered *D.*
472 *melanogaster* TRPA1-C/D to be homologous to *Scaptomyza* TRPA1-CL/DL because of
473 their sequence similarity). We first found that basic properties of each TRPA1 splicing
474 isoform type were highly conserved across species. TRPA1-CL was characterized by
475 activation at lower AITC concentrations and acute spike-like responses at higher
476 concentrations (Figures 4B-4D; Figure S12). By contrast, TRPA1-DL was largely
477 insensitive to AITC at lower doses, while its activation was greater at higher doses with
478 a slower peaking time than TRPA1-CL (Figures 4E-4G; Figure S12). The cross-isoform
479 differences in chemical sensitivity were also consistent with those previously reported in
480 *D. melanogaster* and *Anopheles gambiae* TRPA1s (Du et al. 2024), suggesting that the
481 functional differentiation among TRPA1 splicing isoforms may be widely conserved
482 throughout the Diptera. Moreover, all canonical splicing isoforms responded to heat
483 stimulation in oocytes, consistent with earlier recordings from *D. melanogaster* cell lines
484 (Gu et al. 2019).

485 Despite some degree of functional conservation, however, we also observed
486 substantial interspecific variation in the activity and the sensitivity of the TRPA1

487 channels to AITC. Among the three focal species we studied, *S. pallida* TRPA1
488 (SpTRPA1) generated the largest normalized currents for both splicing isoform types
489 (Figures 4H and 4I; Table 1). Surprisingly, the weakest activity (i.e., maximum current
490 amplitude) was found for both isoforms of *D. melanogaster* TRPA1 (DmTRPA1; Figures
491 4H and 4I; Table 1), despite the strong behavioral aversion to AITC in this species
492 (Figure 1B). *S. flava* TRPA1 (SfTRPA1) splicing isoforms were as weakly activated as
493 DmTRPA1 at lower doses, but they eventually generated large currents at higher AITC
494 concentrations (Figures 4H and 4I; Table 1). Median effective concentrations (EC_{50})
495 were overall lower in TRPA1-CL isoforms than in TRPA1-DL isoforms (Table 1),
496 consistent with visual observations of current traces (Figure 4B-4G). In both isoforms,
497 SfTRPA1 showed larger EC_{50} values against AITC than SpTRPA1 (Table 1).
498 DmTRPA1-C was by far the most sensitive channel among TRPA1-CL isoforms (Table
499 1).

500 Because our current normalization relied on the sizes of heat-evoked currents, it
501 was possible that a channel with a weaker heat activation (I_{Heat}) was represented with
502 larger normalized currents (I_{AITC}/I_{Heat}). This relationship was partially observed for
503 TRPA1-CL isoforms, where SpTRPA1-CL exhibited significantly weaker heat currents
504 than the other two homologous channels (Figure S13; Table 1). However, these
505 differences in heat-evoked currents did not fully explain their variation in chemical
506 sensitivity. For instance, the difference of the maximum normalized currents between
507 DmTRPA1-C and SpTRPA1-CL (4.28-fold difference; Figure 4H; Table 1) was much
508 greater than that of heat currents (1.87-fold difference; Figure S13; Table 1), which
509 alone did not resolve the cross-species variation in normalized currents. We did not
510 observe significant differences in heat currents among TRPA1-DL isoforms (Figure 4K).
511 We concluded that the observed cross-species differences in the activity of TRPA1
512 isoforms still hold true even after taking into account their variation in heat activation.

513 Taken together, SfTRPA1 indeed showed lower sensitivity to AITC and a smaller
514 current amplitude in response compared with SpTRPA1, which suggests that the
515 physiology of the TRPA1 channel evolved concurrently with the transition to herbivory in
516 the *S. flava* lineage and shaped the weak electrophile avoidance. However, these
517 physiological differences in TRPA1 function between species did not entirely align with
518 their differences in behavioral aversion towards AITC (Figure 1B), due to the robust
519 activity of SfTRPA1 at the higher AITC concentrations and the weakest current
520 amplitude of DmTRPA1. This suggests that alternative mechanisms may underlie the
521 differences in feeding aversion towards AITC among species.

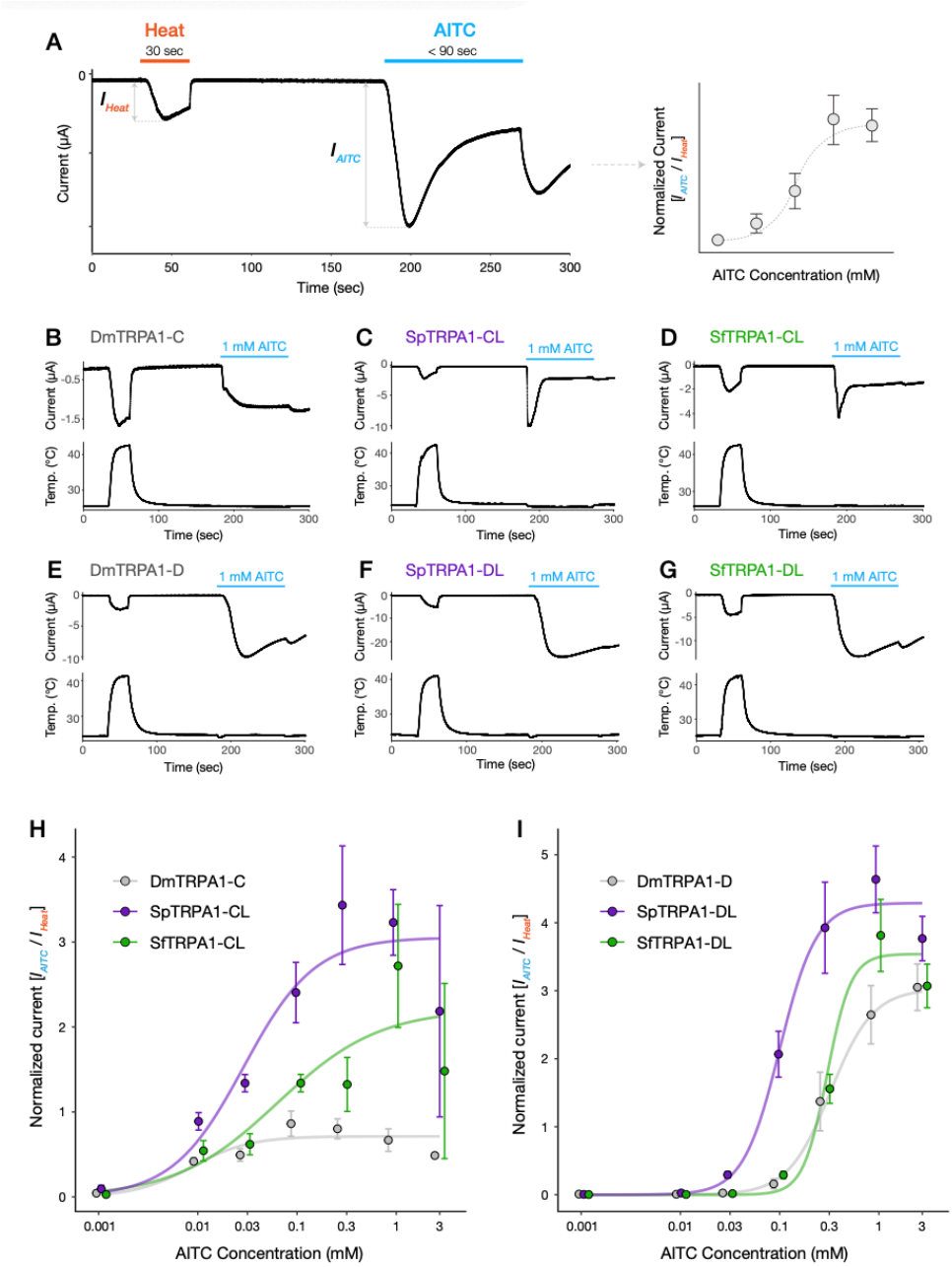

Figure 4. AITC-evoked responses of the TRPA1 channel vary among species. (A) Schematics of electrophysiological recordings and subsequent analysis. A single oocyte was stimulated first by heat (>40 ˚C, 30 seconds) and later by AITC (up to 90 seconds). The peak amplitude of a raw AITC-evoked current (I_{AITC}) was normalized by a heat-evoked current (I_{Heat}), such that a single normalized current (I_{AITC}/I_{Heat}) was obtained for each recording. Data collection was repeated along a dosage series of AITC to visualize the channel's response as a dose-response curve. (B-G) Example current traces of six TRPA1 splicing isoforms analyzed against heat and AITC (1 mM) stimulations. (H) Dose-response curves of three TRPA1-CL splicing isoforms (i.e., DmTRPA1-C, SpTRPA1-CL, and SfTRPA1-CL). Circles represent mean normalized current values at each concentration of AITC (n = 4-10 per group). (I) Dose-response curves of three TRPA1-DL splicing isoforms (i.e., DmTRPA1-D, SpTRPA1-DL, and SfTRPA1-DL). Circles represent mean normalized current values at each concentration of AITC (n = 3-9 per group).

	TRPA1-CL			TRPA1-DL		
	DmTRPA1-C	SpTRPA1-CL	SfTRPA1-CL	DmTRPA1-D	SpTRPA1-DL	SfTRPA1-DL
Maximum normalized current [I_{AITC}/I_{Heat}]	0.714±0.059	3.05±0.34	2.21±0.47	3.03±0.37	4.29±0.29	3.54±0.22
EC_{50} (mM)	0.0086±0.0043	0.029±0.015	0.065±0.055	0.341±0.092	0.103±0.015	0.316±0.031
Mean I_{Heat} (μA)	2.60	1.39	1.82	3.52	4.08	3.32
Number of recordings	35	42	40	31	34	35

Table 1. Summary of electrophysiological recordings from six canonical TRPA1 splicing isoforms. Maximum normalized currents and EC_{50} were predicted values from dose-response curve estimation by drc package (Ritz et al. 2015). Values following the (±) symbol represent standard errors for corresponding parameters.

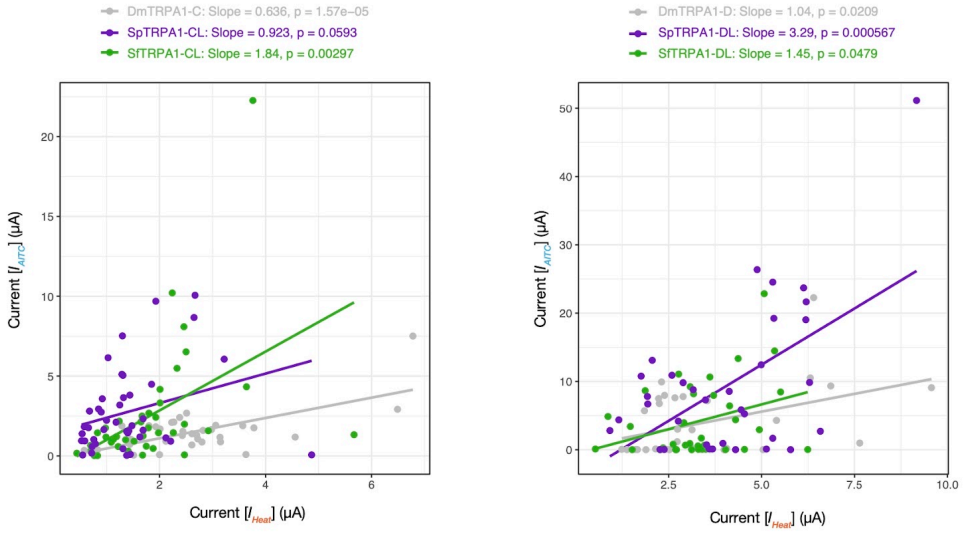

Supplementary Figure S11. Correlations between raw heat-evoked and AITC-evoked currents. Each dot represents a single oocyte. (Left) TRPA1-CL and (Right) TRPA1-DL splicing isoforms.

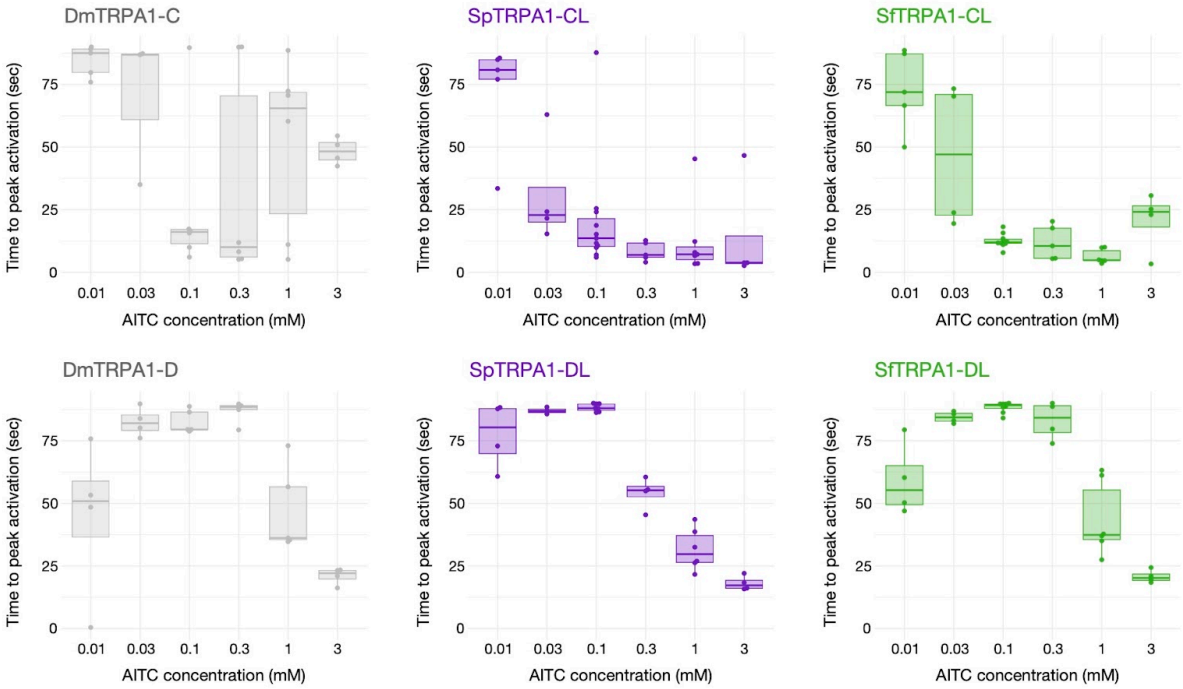

Supplementary Figure S12. Times to reach peak activation in six canonical TRPA1 splicing isoforms. Recordings were carried out within a 90-second AITC stimulation window, across the concentration series from 0.001 mM to 3 mM AITC. Note that the smallest concentration (0.001 mM AITC) was omitted from this analysis due to the lack of observable chemical-invoked currents. Overall, TRPA1-CL(C) isoforms tended to peak faster than TRPA1-DL(D) splicing isoforms.

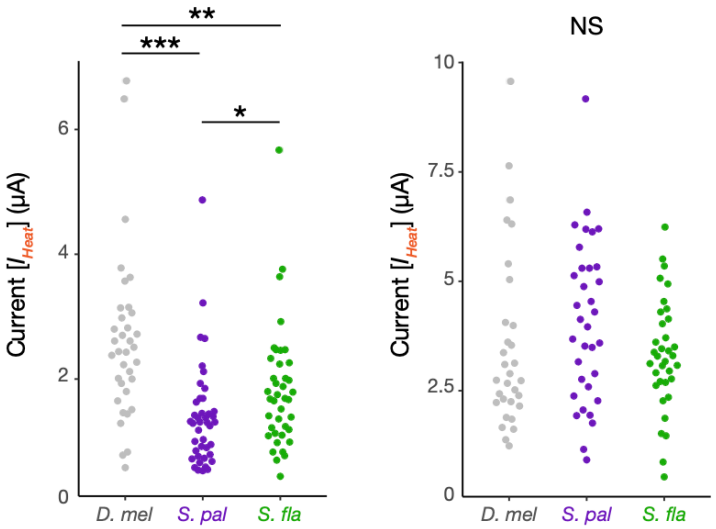

Supplementary Figure S13. Comparisons of raw heat-evoked currents (I_{Heat}). (Left) TRPA1-CL and (Right) TRPA1-DL splicing isoforms, tested by Kruskal-Wallis test and post-hoc Conover's test with Benjamini-Hochberg correction. *: $p < 0.05$, **: $p < 0.01$, ***: $p < 0.001$.

Ectopic expression of TRPA1-CL splicing isoforms partially recapitulates wild-type behaviors

Given the interspecific differences in the physiological responses of the TRPA1 channels to AITC, we next asked whether and to what extent those changes could influence feeding aversion behavior and its evolution. To this end, we designed an *in vivo* genetic rescue experiment using the *GAL4/UAS* system in *D. melanogaster* to test whether *in vivo* expression of TRPA1 isoforms from *Scaptomyza* spp. and *D. melanogaster* can recapitulate the differences in gustatory behaviors between wild-type flies of these species. Using PhiC31-mediated insertion, we created three homozygous *UAS-TrpA1* lines each carrying a full-length copy of *SfTrpA1-CL*, *SpTrpA1-CL* or *DmTrpA1-C*, respectively, and drove their expression in bitter-sensing gustatory neurons under the *DmGr66a* promoter (Lee et al. 2009; Weiss et al. 2011) (Figure 5A). *TrpA1-CL* was selected as the focal splicing isoform since it is the only canonical isoform abundantly expressed in all three species (Figure 3B). All *Gr66a-GAL4* and *UAS-TrpA1* lines were initially set to *TrpA1* null (*TrpA1*^{1}) mutant background (Figure S14) and crossed for experiments (Figure 5A). Test genotypes (i.e., *Gr66a>TrpA1*) and control flies (i.e., *UAS-TrpA1/+*) were then phenotyped using the PER assay to evaluate the contributions of ectopic *TrpA1* expression on their electrophile sensitivities. Flies were challenged with a non-volatile electrophile NMM (N-methylmaleimide) as a deterrent, because it invokes a similar gustatory response as AITC but is far less volatile and would not simultaneously risk activating olfactory pathways, which are responsive to volatile ITCs (Matsunaga et al. 2025).

Although all fly mutants had a *TrpA1*-null background, 10 mM NMM was consistently aversive to all control genotypes (Figure 5B). 5 mM NMM showed mixed results: flies of the *TrpA1*^{1} and *UAS-DmTrpA1-C* lines avoided NMM, while flies of other control genotypes did not show clear signs of aversion compared with the 0 mM NMM treatment (Figure 5B). These patterns suggest that the aversion towards NMM was retained in our transgenic lines via unknown TRPA1-independent mechanisms that were also influenced by genetic backgrounds. Nevertheless, we still found that ectopic expression of SpTRPA1-CL clearly and consistently increased the degree of aversion at 5 mM NMM compared with its control strain, while SfTRPA1-CL did not significantly confer a feeding aversion behavior (Figure 5B), a pattern fully consistent with the physiological responses we observed in oocyte electrophysiology (Figure 4H).

To further isolate the contribution of ectopic TRPA1 expression in *D. melanogaster*, we took the ratios of average PER scores between test (*Gr66a>TrpA1*) and control (*UAS-TrpA1/+*) genotypes for each TRPA1 channel and plotted these as dose-responses (Figure 5C). This showed that SfTRPA1-CL conferred weaker electrophile aversion at 5 mM and 10 mM NMM compared with SpTPRA1-CL or DmTRPA1-C (Figure 5C), consistent with a model of phenotypic evolution wherein TRPA1 physiology underlies the attenuated electrophile aversion of *S. flava*. However,

the differences in feeding aversion were much more subtle between *D. melanogaster* flies ectopically expressing SfTRPA1 or SpTRPA1 (Table 2; Figure 5B) than between wild-type *S. flava* and *S. pallida* flies (Table 2; Figure 1B). This mismatch indicates that TRPA1 physiology alone cannot fully recapitulate interspecific feeding preferences. Overall, our genetic rescue experiments showed the importance of TRPA1 channel physiology for the evolution of gustatory behaviors, but also highlighted the presence of additional molecular mechanisms that might contribute to the near-absence of electrophile aversion in *S. flava*.

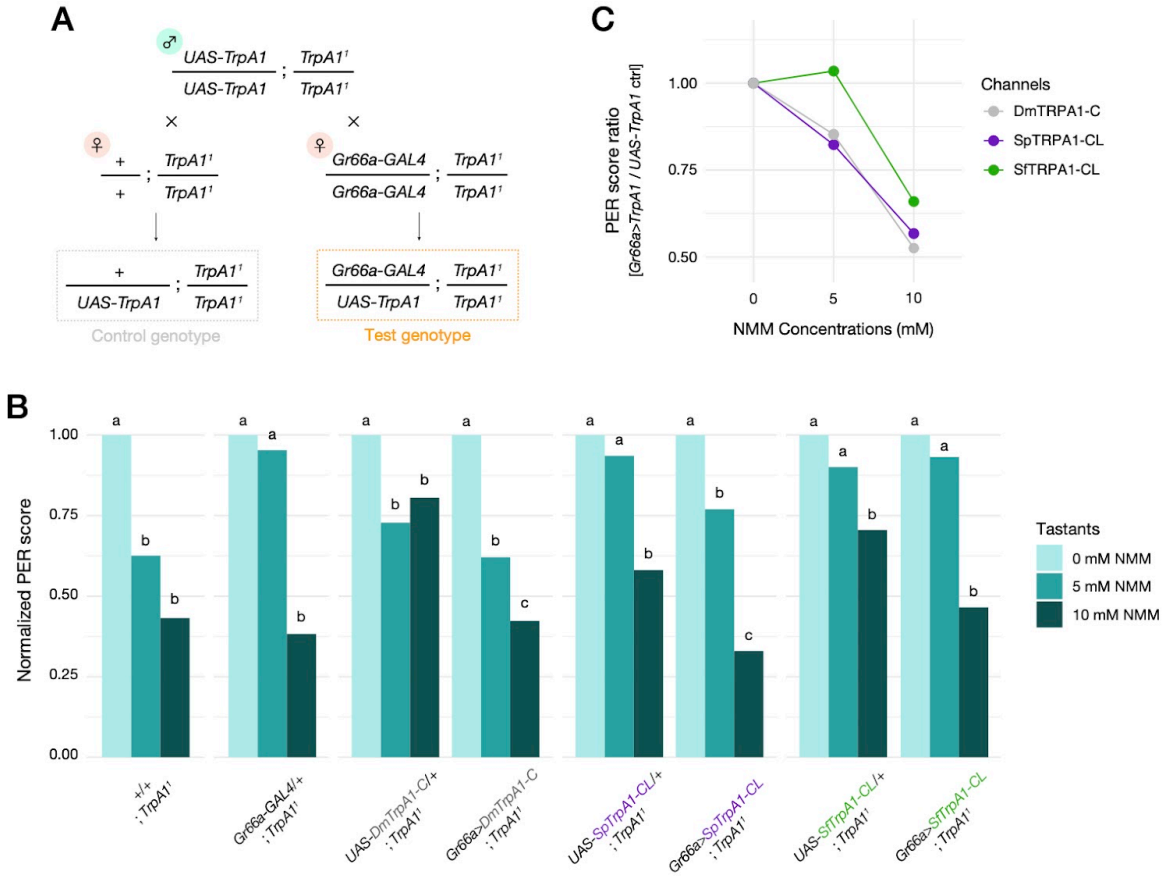

Figure 5. Ectopic expression of *Drosophila/Scaptomyza* TRPA1s partially rescues wild-type behavior. (A) Crossing schemes of *Gr66a>TrpA1* (test group) and *UAS-TrpA1* (control group) flies. Note that all flies were homozygotes of *TrpA1¹* allele that lacked endogenous *dTrpA1* expression. (B) Results of PER assay in eight genotypes across the concentration series of NMM mixed in 100 mM sucrose solution. PER score of a single female fly represents the feeding response to a given tastant over five trials. Bar plots indicate average PER scores for each treatment (n = 15-42) normalized to the score at 0 mM NMM within each genotype. Error bars based on pre-normalized individual PER scores were not provided because of this treatment. Letters indicate significant differences between NMM concentrations within each genotype, tested by pairwise Wilcoxon rank-sum test with Benjamini-Hochberg correction ($p < 0.05$). (C) Ratios of average PER scores between *Gr66a>TrpA1* line and *UAS-TrpA1/+* line for each TRPA1 channel expressed, plotted as line graphs over the three concentrations of NMM.

Species/Genotype	Tastant	PER_0mM	PER_5mM	PER_10mM
D. melanogaster WT	AITC	1	0.703	0.406
S. pallida WT	AITC	1	0.406	0.198
S. flava WT	AITC	1	1.023	0.867
D. melanogaster (*Gr66a>DmTRPA1-C*;*TrpA1*^{1})	NMM	1	0.621	0.42
D. melanogaster (*Gr66a>SpTRPA1-CL*;*TrpA1*^{1})	NMM	1	0.770	0.330
D. melanogaster (*Gr66a>SfTRPA1-CL*;*TrpA1*^{1})	NMM	1	0.932	0.465

Table 2. Summary of wild-type and transgenic PER assays. Average PER scores normalized to 0 mM AITC or NMM were retrieved from Figure 1B (wild-type) and three rescue genotypes in Figure 5B (transgenic)

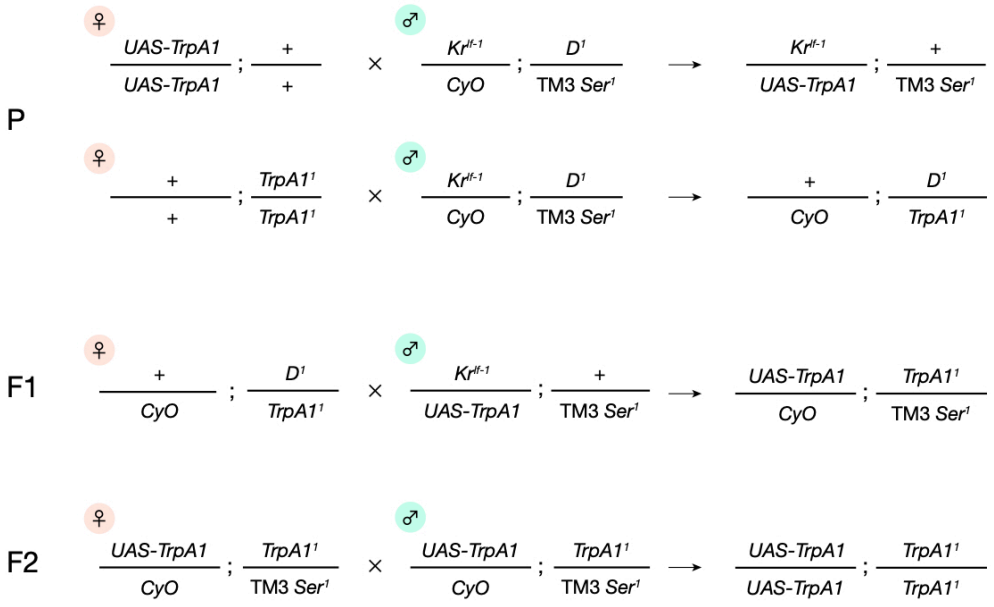

Supplementary Figure S14. Crossing schemes to obtain double homozygotes of *UAS-TrpA1* and *TrpA1*^{1} alleles. A double balancer line (*Kr*$^{lf-1}$/*CyO*;*D*^{1}/TM3 *Ser*^{1}) was utilized to merge two alleles. Only second and third chromosomes are shown. *Gr66a-GAL4*;*TrpA1*^{1} homozygotes were also obtained in the same procedure.

616 **Co-expression of canonical TRPA1 splicing isoforms modulates AITC-evoked**
617 **currents**

618 To search for alternative mechanisms behind sensory adaptation in *S. flava*, we
619 turned our attention to the regulation of alternative splicing of the *TrpA1* gene, inspired
620 by the example from the vampire bat in which a truncated TRPV1 splice variant
621 underlies prey finding behavior (Gracheva et al. 2011). Amplicon sequencing highlighted
622 the difference in expression proportions of the two canonical TRPA1 isoforms,
623 TRPA1-CL and TRPA1-DL, between *S. flava* and *S. pallida* (Figure 3B and 3C). Since
624 these two isoforms exhibited differential sensitivity towards AITC (Table 1; Figure 4H
625 and 4I), we hypothesized that variation in co-expression of canonical TRPA1 isoforms
626 influences the chemical sensitivity of gustatory sensory neurons. To this end, we
627 explored the functional consequences of isoform co-expression, again using *Xenopus*
628 oocyte electrophysiology. By taking advantage of direct RNA injection into oocytes, we
629 were able to precisely manipulate the compositions of TRPA1 isoforms expressed in a
630 cell by pre-mixing multiple mRNAs at a particular ratio. For initial experiments, we
631 prepared canonical *TrpA1* mRNA mixtures in integer ratios that best represented our
632 observations from amplicon sequencing (Figure 3B; i.e., *S. flava* labella CL:DL=7:6, *S.*
633 *pallida* labella CL:DL=5:2, *S. flava* tarsi CL:DL=1:7, *S. pallida* tarsi CL:DL=6:7).

634 As a result, we found that cells responded more actively at lower AITC
635 concentrations as the proportion of TRPA1-CL, an isoform with a higher chemical
636 sensitivity, increased in both species (Figure 6A and 6B). By contrast, enrichment of the
637 TRPA1-DL isoform decreased the current amplitudes at low AITC concentrations
638 (Figure 6A and 6B). These patterns were consistent with our working hypothesis and
639 showed that co-expressed TRPA1 isoforms additively modulated the current response
640 of cells and potentially of gustatory neurons.

641 Using the same dataset, we further compared the normalized responses of
642 labella- and tarsi-mimicking mixtures between *S. flava* and *S. pallida*. We found that *S.*
643 *flava* TRPA1 mixtures yielded significantly weaker responses than *S. pallida* at 0.1 mM
644 AITC in both mixtures (Figures 6C and 6D), consistent with the weaker current
645 amplitudes of SfTRPA1 than of SpTRPA1 (Figures 4H and 4I). Intriguingly, the degree of
646 interspecific difference varied at 0.01 mM AITC: responses of oocytes were significantly
647 greater for labellar mixtures of *S. pallida* than of *S. flava* (Figure 6C), while those for
648 tarsal mixtures did not differ between species (Figure 6D). The relative inactivity of *S.*
649 *flava* labellar mixture at 0.01 mM was likely achieved through the higher proportion of
650 TRPA1-DL in this mixture compared with its *S. pallida* counterpart (Figure 3B and 3C).
651 This pattern shows that species-specific or tissue-specific regulation of alternative
652 splicing could indeed drive sensory differentiation among drosophilids with divergent
653 dietary needs. Overall, our results with mRNA mixtures that phenocopied the native
654 isoform ratios in labella and tarsi of flies from different species provide a model for how

the physiological response of the sensory neurons can be modulated through differential regulation of TRPA1 isoforms.

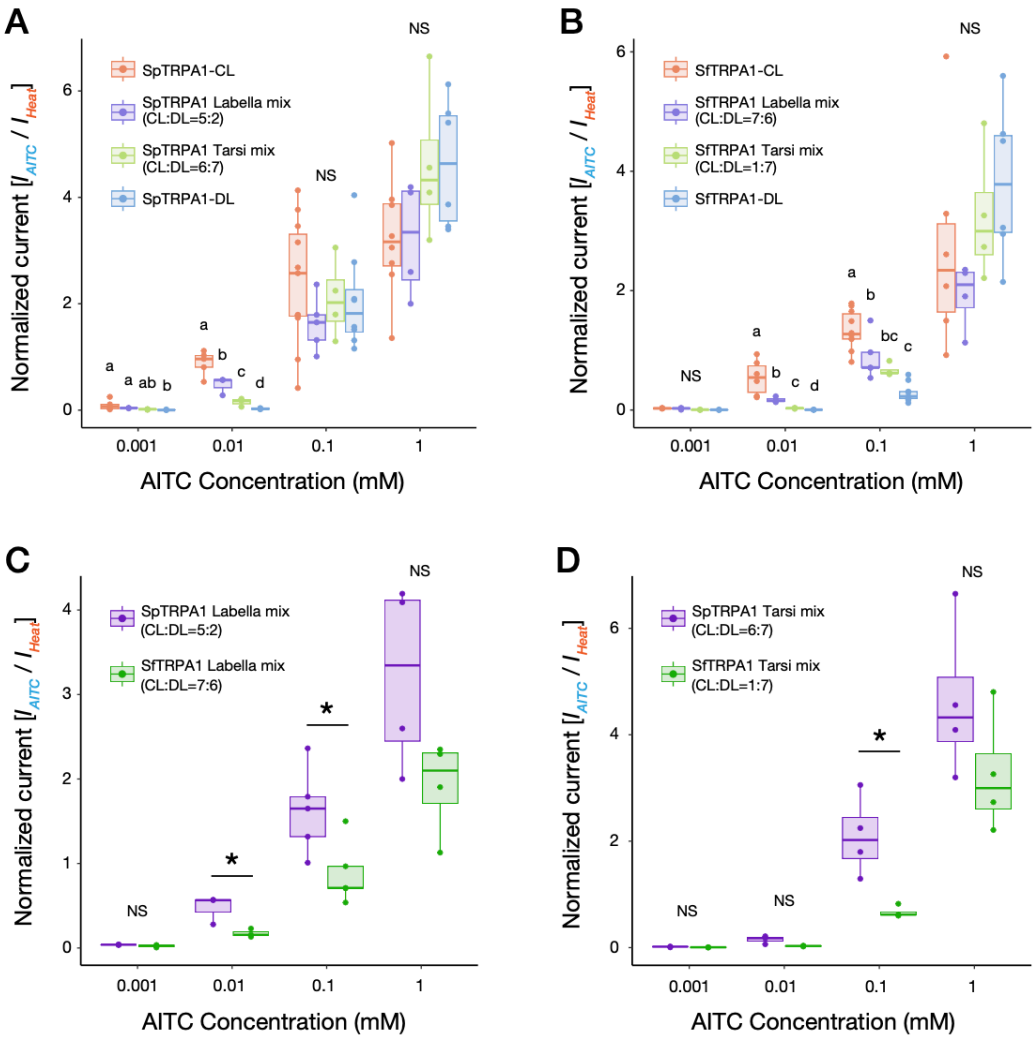

Figure 6. Co-expression of canonical TRPA1 isoforms additively modulates electrophile-evoked responses. (A, B) Heat-normalized AITC-evoked currents of (A) *S. pallida* TRPA1 mixtures (n = 3-11) and (B) *S. flava* TRPA1 mixtures (n = 3-10) at the four concentrations of AITC. Differences between isoforms were tested by one-way ANOVA followed by post hoc Tukey's post hoc test (0.1 and 1 mM AITC) or Kruskal-Wallis test followed by post hoc Conover's test (0.001 and 0.01 mM AITC) with Benjamini-Hochberg correction. Letters indicate the significant differences of the mean between groups at each concentration ($p < 0.05$). (C, D) Heat-normalized AITC-evoked currents of RNA mixtures mimicking (C) labellar *TrpA1* expression (n = 3-5 per group) and (D) tarsal *TrpA1* expression (n = 3-4 per group), using the same datasets from (A) and (B). Differences between species at each concentration were tested by Student's t-test or Welch's t-test. *: $p < 0.05$.

Co-expression of inactive TRPA1 isoforms attenuates AITC-evoked currents

Our amplicon sequencing also revealed two underrepresented TRPA1 isoforms from *S. flava*, SfTRPA1-CS and SfTRPA1-DS (Figures 3B and 7A). We investigated the characteristics of these minor TRPA1 channel variants and found that their responses to AITC or heat stimulations were substantially weaker than those of canonical isoforms, even at the highest AITC concentrations (Figure 7C; Figure S15). Likewise, a minor isoform in *S. pallida*, SpTRPA1-EL, barely responded to both stimuli (Figure 7B), consistent with its homology to the DmTRPA1-E isoform with a similar non-responsive phenotype (Gu et al. 2019).

We next investigated how these "inactive" TRPA1 isoforms may affect the physiology of sensory neurons based on oocyte electrophysiology. To simply evaluate the contributions of the inactive TRPA1s, we created 1:1 mRNA mixtures of both an inactive and a canonical TRPA1 isoform (i.e., TRPA1-CL) for *S. flava* and *S. pallida*, and compared their responses to single-isoform recordings. We found that the activity of the 1:1 mixtures fell in between those from the inactive and the canonical isoforms in both species (Figures 7D and 7E), indicating that the presence of inactive TRPA1 isoforms simply lowers the neuronal response to AITC in an additive manner. Since the proportion of inactive splicing isoforms in labella was greater in *S. flava* than in *S. pallida* or in *D. melanogaster* (Figure 7F), it is possible that these inactive TRPA1 channels play an additional role in causing the evolutionary divergence of gustatory behavior among these species.

Taken together with the data from canonical isoform mixtures, these *in vitro* experimental manipulations revealed that the enriched expression of a particular TRPA1 splicing isoform will shift the cellular response towards the phenotype conferred by this isoform, whether that is towards higher or lower sensitivity to AITC stimulation. We speculate that these results could directly influence the observed differences between species (and organs) in mediating gustatory avoidance behaviors of flies towards AITC.

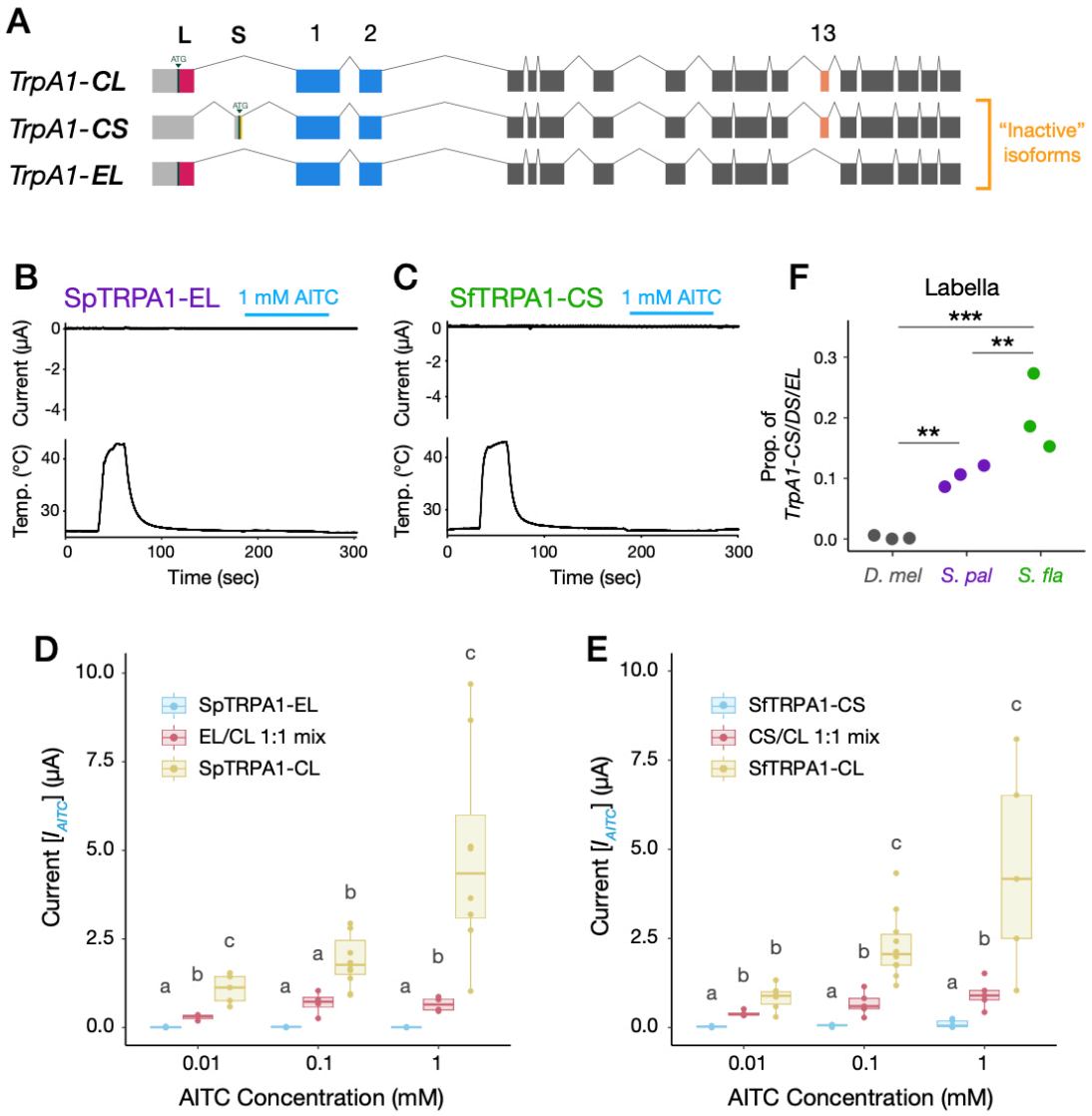

Figure 7. Co-expression of "inactive" TRPA1 isoforms reduces electrophile-evoked responses. (A) Exonic structures of *Scaptomyza TrpA1-CL* and two "inactive" isoforms, *TrpA1-CS* and *TrpA1-EL*. Green small arrowheads indicate putative translation start sites, whose upstream are putative 5'UTRs (pale colored). (B, C) Example current traces of (B) SpTRPA1-EL and (C) SfTRPA1-CS stimulated by heat and 1 mM AITC. (D, E) Comparisons of raw AITC-evoked current amplitudes between TRPA1-CL, an inactive TRPA1 isoform (either TRPA1-EL or -CS), and a 1:1 mixture of the two isoforms from (D) *S. pallida* (n = 3-11) and (E) *S. flava* (n = 4-10). Letters indicate the statistical differences in the mean current amplitudes at each AITC concentration using Kruskal-Wallis test followed by post-hoc Conover's test with Benjamini-Hochberg correction ($p < 0.05$). (F) Relative abundances of all inactive isoforms together (i.e., *TrpA1-CS*+*TrpA1-DS*+*TrpA1-EL*) in labellar cDNA, based on the data from Fig. 3B (n = 3 per species). Variation in splicing isoform compositions among species was modeled by GLM with Gaussian distribution, and further tested by Tukey's post-hoc test with Benjamini-Hochberg correction. **: $p < 0.01$, ***: $p < 0.001$.

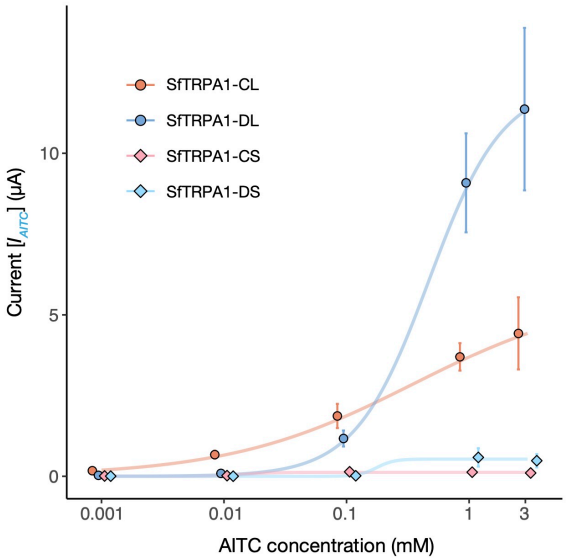

Supplementary Figure S15. Dose-response curves of the four SfTRPA1 isoforms. Note that the prediction of dose-response was performed on raw current values (I_{AITC}), instead of normalized values (I_{AITC}/I_{Heat}), because weak heat activation of the inactive isoforms prevented proper normalization. n = 3-12 per group.

DISCUSSION

Niche shifts in animals are often coupled with the evolution of behavioral traits (Duckworth 2009), but the molecular mechanisms underlying such events remain elusive. Chemosensory traits are good candidates for exploring this problem because of their relative simplicity and the modularity of their functional units. Here, we investigated the evolutionary, genetic, and molecular basis of differences in gustatory behavior between a recently-derived specialist herbivore, *Scaptomyza flava*, and its microbe-feeding relatives, *S. pallida* and *Drosophila melanogaster*. Importantly, the *Scaptomyza* genus is nested phylogenetically within the paraphyletic subgenus *Drosophila*, which includes the Hawaiian *Drosophila* as well as species such as *D. mojavensis* and *D. virilis*. Thus, species of *Scaptomyza* are of comparable phylogenetic distance from the genetic model species *D. melanogaster* as these congeners. By focusing on the TRPA1 channel, a primary transducer of information presented by electrophilic compounds such as mustard-derived ITCs, which are so important in the niche shift of *S. flava* to GLS-bearing plants, we aimed to decipher the genetic and molecular mechanisms associated with behavioral evolution in this mustard-plant specialist. Specifically, we hypothesized that *S. flava* has evolved a weaker gustatory aversion against ITCs and that some combination of changes in the expression, protein sequence, and regulation of alternatively spliced transcripts of the *TrpA1* gene contributed to this reduction in avoidance to ITCs.

Our behavioral assay revealed significantly attenuated feeding aversion against allyl isothiocyanate (AITC) in *S. flava*, likely mediated by changes in the gustatory circuit (Figure 1B). However, the *S. flava* genome maintains an intact *TrpA1* gene and the *S. flava* TRPA1 (SfTRPA1) channel is functionally conserved as an electrophile-gated ion channel like its orthologues in *D. melanogaster* and *S. pallida* (Figure 4H and 4I). We previously reported the entire loss of behavioral attraction to yeast odor in *S. flava* and the associated losses of genes encoding receptors tuned to these volatiles, along with their dietary transition from microbe feeders to mustard specialists (Goldman-Huertas et al. 2015). Such extreme chemosensory loss was not the case for gustatory aversion towards ITCs, likely because fly TRPA1 also mediates detection of a wide array of nociceptive stimuli and its loss would be immediately deleterious (Himmel and Cox 2020). Another functional conservation of TRPA1 is the physiological difference between splicing isoforms. Functional diversity among *D. melanogaster* TRPA1 (DmTRPA1) splicing isoforms has been documented elsewhere (Kang et al. 2012; Zhong et al. 2012; Gu et al. 2019; Leung et al. 2020; Gu et al. 2022; Du et al. 2024). Isoform DmTRPA1-C and its homologs are consistently described as channels more sensitive to chemicals compared with isoform DmTRPA1-D and its homologs (Leung et al. 2020; Du et al. 2024) We found that such differences in dose dependency and peak activation time were also conserved between two “canonical” TRPA1 splicing isoforms

748 of *S. flava*, TRPA1-CL and -DL (Figure 4H and 4I; Figure S12). Although canonical
749 *Scaptomyza TrpA1s* recruited a new exon at the N-terminus (Exon L; Figure 3A), this
750 alone does not confer a novel response property to the channel based on our
751 experiments.

752 Despite a high degree of conservation, we discovered some salient physiological
753 differences between *S. flava* TRPA1 (SfTRPA1) and *S. pallida* TRPA1 (SpTPRA1) that
754 could be associated with adaptation to mustard plants. Notably, SfTRPA1 exhibited a
755 lower amplitude of ionic currents and a lower electrophile sensitivity in both canonical
756 isoforms compared with SpTRPA1 (Figure 4H and 4I; Table 1). Such physiological shifts
757 in the TRPA1 channel would decrease firing rates of peripheral gustatory neurons
758 against ITCs and thus reduce behavioral aversion, consistent with *S. flava*'s
759 mustard-feeding ecology. Genetic rescue experiments in *D. melanogaster* further
760 recapitulated the behavioral variation across species, wherein SpTRPA1-CL conferred a
761 larger degree of electrophile aversion compared with SfTRPA1-CL (Figure 5B and 5C).
762 These results are consistent with our working hypothesis that changes in TRPA1
763 channel physiology can drive behavioral divergence. Although we did not attempt to
764 infer ancestral character states of TRPA1 prior to the specialization onto mustards,
765 Kang and colleagues (Kang et al. 2010) compared the chemical responses of the
766 TRPA1-D isoform (called "TRPA1(A)" in their paper) of *D. mojavensis* and *D. virilis* to
767 that of *D. melanogaster*. Despite some differences in the recording scheme, those
768 authors reported an EC_{50} value for DmTRPA1-D similar to our observation (0.278±0.024
769 mM (Kang et al. 2010); 0.341±0.092 mM (this study, Table 1)), while EC_{50} values for the
770 other two species indicated higher sensitivity to chemicals, comparable to our
771 observation for SpTRPA1-DL (i.e., DmojTRPA1-D: 0.121±0.013 mM, DvirTRPA1-D:
772 0.108±0.012 mM (Kang et al. 2010); SpTRPA1-DL: 0.103±0.015 mM (This study, Table
773 1)). A parsimonious interpretation is that the TRPA1-DL(D) isoform was already
774 sensitized in the most recent common ancestor of the subgenus *Drosophila* (which
775 includes *Scaptomyza*) and later desensitized only in the *S. flava* lineage. These patterns
776 indicate that the physiological evolution of TRPA1 coincided with, and potentially
777 facilitated, the dietary transition to mustards and other Brassicales plants.

778 Altogether, results from our *in vitro* and *in vivo* experiments support the
779 hypothesis that physiological changes to the sensitivity of the TRPA1 channel to
780 electrophiles like AITC in part underlie gustatory evolution in *S. flava* (Figure 8).
781 Although causal amino acid substitutions behind the physiological evolution of SfTRPA1
782 remain unidentified, the conservation of cysteine residues that trigger channel gating,
783 which underwent substitutions in TRPA1 from the pain-insensitive African mole-rat
784 (Eigenbrod et al. 2019), indicates that natural selection targeted another domain of the
785 channel. Alternatively, herbivore-specific substitutions in ankyrin repeat domains (ARDs)
786 could potentially modify regulation of TRPA1 channel gating via structural changes of

ARDs as previously suggested (Cordero-Morales et al. 2011; Saito et al. 2022). Functional consequences of substitutions in ARDs warrant further investigation.

However, TRPA1 physiology alone does not explain the overall behavioral differences between fly species, as illustrated by the small degree of phenotypic divergence between the transgenic *D. melanogaster* strains expressing *TrpA1* isoforms of each species (Figure 5B and 5C). Another notable finding is the interspecific variation in the composition of *TrpA1* splicing isoforms (Figure 3) and its modulation of cellular responses to sensory stimuli *in vitro* (Figure 6 and 7). *TrpA1* isoforms are co-expressed in nociceptive C4da neurons in larval *D. melanogaster* (Gu et al. 2019). Because labellar expression of *S. flava TrpA1* was restricted to a small number of bitter-sensing neurons (Figure 2J-2L), it is reasonable to assume that these *Scaptomyza TrpA1* isoforms are co-expressed in gustatory neurons. Our oocyte electrophysiology after introducing mixtures of TRPA1 channel isoforms with different response properties showed that physiological responses of a cell tend to be closer to those of predominantly expressed isoforms (Figure 6 and 7). We discovered that the isoform compositions that mimicked labellar *TrpA1* expression patterns of *S. flava* and *S. pallida* produced different responses to a lower AITC concentration (Figure 6C), while the tarsal-mimicking *TrpA1* mixtures did not show a difference (Figure 6D). This suggests that isoform composition of TRPA1 channels allows fine-tuning of the dose-dependency of gustatory neurons and that the regulation of these isoforms could therefore be subject to natural selection depending on the species-specific or tissue-specific needs.

We propose that proportionally higher expression of TRPA1-DL, a less electrophile-sensitive isoform, could be another mechanism facilitating the observed evolutionary change in diet within the *S. flava* lineage, because it would suppress feeding aversion towards Brassicales plants through the reduced activity of ITC-sensing neurons at low chemical concentrations (Figure 8). Proportionally higher expression of TRPA1-CL, on the other hand, would sensitize ITC-sensing neurons and could have been favored in non-mustard-feeding species like *S. pallida* to prevent them from consuming electrophilic toxins (Figure 8). This model is analogous to the enrichment of a heat-sensitive TRPV1 isoform in the vampire bat, which likely enables the sensation of infrared emitted by its mammalian prey (Gracheva et al. 2011). Expression of "inactive" TRPA1 isoforms, such as SfTRPA1-CS or SpTRPA1-EL, could further reduce sensitivity of ITC-sensing neurons, as their presence in isoform mixtures proportionately reduced current amplitudes against stimulation (Figure 7). A higher proportion of these inactive isoforms in *S. flava* than in *S. pallida* (Figure 7F) could thus also have contributed to the attenuation of bitter-sensing neurons against ITCs in the *S. flava* lineage. Taken together, our results suggest that the evolution of *TrpA1* isoform composition is another molecular mechanism associated with the ecological shift to Brassicales host plants in *S. flava*, likely occurring in parallel with the evolution of TRPA1 channel physiology.

827 One of our surprising findings is that DmTRPA1s produced the smallest current
828 amplitude among the three species (Figure 4H and 4I) despite the strong feeding
829 aversion for ITCs in *D. melanogaster* (Figure 1B). This apparent contradiction could be
830 explained by taking into account both gene expression and physiology. First, the labellar
831 expression level of *D. melanogaster TrpA1* was by far the highest among the three
832 species (Figure 2A-2C). Second, *D. melanogaster* labella almost entirely lacked the
833 expression of inactive *TrpA1* isoforms (Figure 3B). Lastly, the EC_{50} of DmTRPA1-C,
834 which is the dominant isoform in *D. melanogaster* labella, was much lower than
835 homologues in the other two species (Table 1). These findings together indicate that *D.*
836 *melanogaster* achieves robust electrophile aversion by enriching its bitter-sensing
837 neurons with a higher number of sensitive TRPA1 channels to compensate for the weak
838 activity of each single channel (Figure 8). This is yet another example wherein the
839 combination of channel physiology and gene expression of TRPA1 may explain
840 behavioral variation. Our dataset also highlights the perils of using *D. melanogaster* as a
841 "default" or baseline species and the benefits of using taxa representing a phylogenetic
842 gradient.

843 HCR RNA-FISH showed that *TrpA1* expression was restricted to bitter-sensing
844 neurons in the *S. flava* labellum, indicating that ITCs serve as gustatory deterrents even
845 for this mustard feeder (Figures 2G-L). This pattern reflects the dual aspects of ITCs for
846 specialized herbivores: although volatile ITCs serve as host-associated cues (token
847 stimuli) that allow specialist herbivores to find their food and oviposition sources (Finch
848 1978; Wallbank and Wheatley 1979; Matsunaga et al. 2022), they are still toxins that
849 can delay development and will result in lethality at high doses (Lichtenstein et al. 1964;
850 Whiteman et al. 2011). Rather than switching the valence of ITC perception to full
851 acceptance, the mustard specialist *S. flava* appears to have fine-tuned the strength of
852 bitter sensing-neuron activity so that it does not trigger aversion unnecessarily. On the
853 other hand, the high *TrpA1* expression in *S. flava* tarsi was unexpected. Leg gustatory
854 neurons of the flies serve as a gateway to assess the quality of a potential food source,
855 in which plant secondary metabolites are usually perceived as aversive stimuli (Scott
856 2018). However, some butterflies are known to perceive specific host plant-derived
857 chemicals through their chemosensory neurons in the legs as attractive
858 oviposition-stimulating cues, such as GLSs for the cabbage white (*Pieris rapae*) (Huang,
859 Renwick et al. 1993a; Huang et al. 1993b; Yang et al. 2021) and synephrine for the
860 Asian swallowtail (*Papilio xuthus*) (Nishida et al. 1987; Ozaki et al. 2011; Ryuda et al.
861 2013). Robust *TrpA1* expression in the tarsi could potentially allow for more precise
862 evaluation of host plant quality for *S. flava*.

863 In summary, our work demonstrates how evolution of *TrpA1* shapes behavioral
864 variation across drosophilid flies through a combination of differences in overall
865 expression levels, protein evolution, and compositional modulation of functionally
866 diverse splicing isoforms. The latter two mechanisms are prominent contributors to the

attenuated aversion of *S. flava* towards dietary electrophiles (Figure 8). To our knowledge, this is the first chemosensory example in which alternative splicing of sensory channel genes drives the evolution of novel behavior. While changes in receptor sensitivity are commonly observed in other cases of sensory evolution (Gracheva et al. 2010; McBride et al. 2014; Prieto-Godino et al. 2017; Eigenbrod et al. 2019; Auer et al. 2020; Brand et al. 2020; Capek et al. 2025) alongside gains and losses of receptor genes (McBride 2007; McBride and Arguello 2007; Goldman-Huertas et al. 2015; Matsunaga et al. 2022; Peláez et al. 2023), alternative splicing has been rarely associated with sensory novelty except for the case of TRPV1 in the infrared-sensing vampire bat (Gracheva et al. 2011). This contrast can be interpreted through the lens of evolutionary constraint: large-effect mutations in functionally modular gene families, like most insect chemoreceptors, can easily pass through the selective sieve and remain in a population, while such mutations in conserved and more pleiotropic genes are more maladaptive and therefore rarely observed as segregating or as substitutions. When evolutionary novelty arises through changes in highly conserved genes, one solution is gene duplication, which allows for retention of a functional copy of a gene to mitigate fitness costs from new mutations in the other copy, as seen in the parallel evolution of neurotoxin resistance via duplication of the insect GABA receptor gene *Rdl* (Guo et al. 2023). Similarly, modulation of alternative splicing may offer flexibility as the population explores a novel fitness landscape while maintaining the core gene functions. A prediction flowing from this is that alternative splicing provides avenues for the evolution of novel protein sequences for genes under strong constraint. Long-read sequencing technology and the tools of model organisms for detailed functional experiments are now allowing for discovery of yet another mechanism through which adaptive phenotypic evolution can occur. Our findings suggest that additional research on alternative splicing as a potential mechanism underlying adaptation is likely to be fruitful.

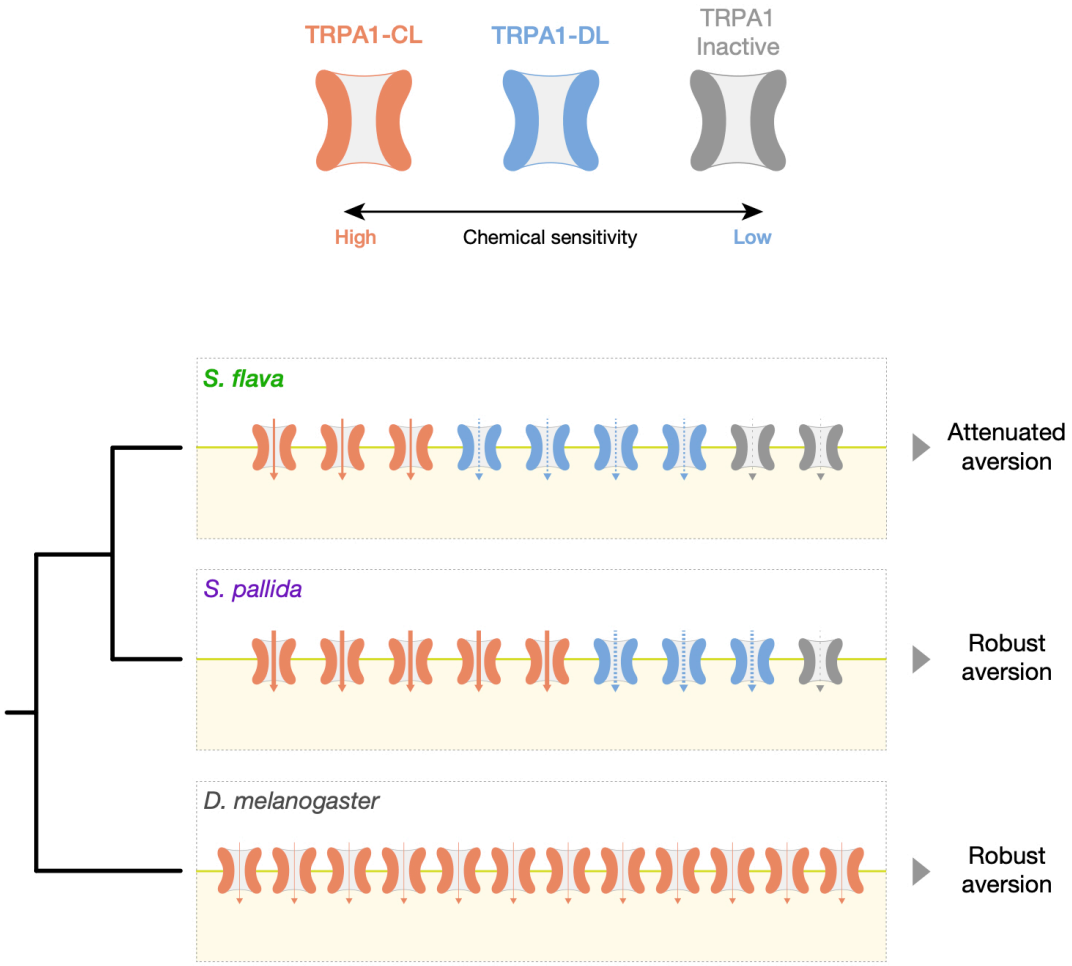

Figure 8. A model of sensory evolution through the combinatorial molecular changes of TRPA1 based on the results of our study. The diagram illustrates the expression patterns of TRPA1 channels in (labellar) gustatory neurons. Thickness and density of dashed arrows represent the activity of each TRPA1 isoform (i.e., degree of positively charged currents conducted by the channels) at lower ITC concentrations. Numbers of ion channels indicate the absolute expression level of *TrpA1* and the relative expression of splicing isoforms. Our analyses suggest that the weak electrophile aversion of *S. flava* is primarily attributed to the desensitization to chemical stimulus and the enrichment of less sensitive splicing isoforms of the TRPA1 channel, compared with the microbe-feeding relative *S. pallida*. In microbe-feeding *D. melanogaster*, which has the highest overall *TRPA1* gene expression levels and highest enrichment of sensitive splicing isoforms, likely compensate for the weakest activity of its TRPA1 channel and maintains its robust aversion against ITCs.

904 **KEY RESOURCES TABLE**

905

REAGENT or RESOURCE	SOURCE	IDENTIFIER
Experimental models: Organisms/Strains		
Scaptomyza flava	Lab colony; Originally collected from Portsmouth, NH (USA)	
Scaptomyza pallida	Lab colony; Originally collected from Berkeley, CA (USA)	
Drosophila melanogaster Canton-S	Gift from Kristin Scott lab	
Arabidopsis thaliana Col-0	ABRC (Columbus, OH, USA)	
Xenopus laevis	Hamamatsu Seibutsu Kyozai (Hamamatsu, Japan)	N/A
D. melanogaster, *pGr66a-GAL4*;*Gr93a*^{3}	Bloomington Stock Center	#28801
D. melanogaster, *w**;*TrpA1*^{1}	Bloomington Stock Center	#26504
D. melanogaster, *w**;*CyO/Krlf-1*;*TM3,Ser1/D*^{1}	Bloomington Stock Center	#7198
D. melanogaster, *w*^{1118}	Gift from Kristin Scott lab	
D. melanogaster, *UAS-SfTrpA1-CL* (attp40)	This study	N/A
D. melanogaster, *UAS-SpTrpA1-CL* (attp40)	This study	N/A
D. melanogaster, *UAS-DmTrpA1-C* (attp40)	This study	N/A
Chemicals, peptides, and recombinant proteins		
Allyl Isothiocyanate (AITC)	Sigma-Aldrich	Catalog #377430
Sucrose	Thermo Fisher Scientific	Catalog #S5500
Agarose	Sigma-Aldrich	Catalog #A9539
Triton X-100	Thermo Fisher Scientific	Catalog #85111
PBS (10X), pH 7.4	Thermo Fisher Scientific	Catalog #70011044
16% Paraformaldehyde	Thermo Fisher Scientific	Catalog #28908
NaCl	Any	N/A
KCl	Any	N/A
$CaCl_2$	Any	N/A
$MgCl_2$	Any	N/A
HEPES	Any	N/A
DMSO	Any	N/A
N-methylmaleimide (NMM)	Sigma-Aldrich	Catalog #389412
Critical commercial assays		
Reliaprep RNA Tissue Miniprep System	Promega	Catalog #Z6111
Biomasher Standard homogenizer	Takara Bio Inc.	Catalog #9791A
Qubit RNA High Sensitivity Kit	Thermo Fisher Scientific	Catalog #Q32852

Kapa RNA HyperPrep Kit	Roche Sequencing	Catalog #KK8540
Bioanalyzer High Sensitivity DNA Kit	Agilent Technologies	Catalog #50674626
HCR™ RNA-FISH Kit	Molecular Instruments Inc.	N/A
SuperScript IV First-Strand Synthesis System	Invitrogen	Catalog #18091050
Phusion High-Fidelity DNA Polymerase	New England Biolab	Catalog #M0530S
Monarch DNA Gel Extraction Kit	New England Biolab	Catalog #T1020
LongAmp Taq 2X Master Mix	New England Biolab	Catalog #M0287S
PCR Barcoding Expansion (EXP-PCB001)	Oxford Nanopore Technologies	
QIAquick PCR Purification Kit	Qiagen	Catalog #28104
Qubit dsDNA Broad Range Assay Kit	Thermo Fisher Scientific	Catalog #Q32850
SPRIselect	Beckman Coulter	Catalog #B23317
Ligation Sequencing Kit (SQK-LSK109)	Oxford Nanopore Technologies	
Flongle Flow Cell (R9.4.1)	Oxford Nanopore Technologies	
MinION Mk1B	Oxford Nanopore Technologies	
NEBuilder HiFi DNA Assembly Master Mix	New England Biolab	Catalog #E2621S
AflII	New England Biolab	Catalog #R0520L
NotI-HF	New England Biolab	Catalog #R3189L
RsrII	New England Biolab	Catalog #R501S
EcoRI-HF	New England Biolab	Catalog #R3101L
mMessage mMachine SP6 Transcription Kit	Thermo Fisher Scientific	Catalog #AM1340
Collagenase A	Roche	Catalog #C756V80

Oligonucleotides

Supplementary Table

Recombinant DNA

Plasmid: pOX(+)	(Dowland et al. 2000)
Plasmid: pUAST::attB	(Bischof et al. 2007)
S. flava TrpA1-CL cDNA	Artificial synthesis (Genscript)
S. flava TrpA1-DL cDNA	Artificial synthesis (Genscript)
S. flava TrpA1-CS cDNA	*S. flava* adult labella
S. flava TrpA1-DS cDNA	*S. flava* adult labella
S. pallida TrpA1-CL cDNA	*S. pallida* adult labella
S. pallida TrpA1-DL cDNA	*S. pallida* adult tarsi
S. pallida TrpA1-EL cDNA	*S. pallida* adult labella
D. melanogaster TrpA1-C cDNA	*D. melanogaster* third-instar larva whole body
D. melanogaster TrpA1-D cDNA	Gift from Marco Gallio lab

Software and algorithms

R v4.2.1

Rstudio	
survminer v0.4.9	(Kassambara et al. 2017)
Fastp v0.21.0	(Chen et al. 2018)
STAR v2.7.1a	(Dobin et al. 2013)
Trim Galore v0.6.6	
HTseq v0.9.1	(Anders et al. 2015)
BLAST v2.10.1	
DESeq2 v1.36.0	(Love et al. 2014)
ashr	(Stephens 2017)
Trinity v2.5.1	(Grabherr et al. 2011)
MAFFT v7.273	(Katoh and Standley 2013)
IGV v2.9.4	(Thorvaldsdóttir et al. 2013)
MinKNOW v22.12.7	Oxford Nanopore Technologies
Guppy v6.4.6	Oxford Nanopore Technologies
AlphaFold Server	(Abramson et al. 2024)
pCLAMP Software Suite	Molecular Devices
drc v3.0-1	(Ritz et al. 2015)

Other

Supplementary Table

906

METHOD DETAILS

Fly strains. The *Scaptomyza flava* laboratory colony was originally established from >150 wild larvae collected from Portsmouth, NH (USA) in 2008. The colony was maintained in cages containing *Arabidopsis thaliana* Col-0 strain as larval and adult food source at 20-21°C and 60% relative humidity (RH) in a walk-in environmental room on a 12L:12D cycle. The *Scaptomyza pallida* lab colony was an isofemale line established from a wild female fly collected at the University of California, Berkeley campus (CA, USA) in 2017. The colony was reared on organic spinach (purchased at Trader Joe's, CA, USA) placed on top of molasses-cornmeal media purchased from UC-Berkeley Fly Food Facility. Other rearing conditions were identical to those of *S. flava* colony. Wild-type and transgenic *Drosophila melanogaster* lines were obtained from Bloomington Drosophila Stock Center or Kristin Scott lab (University of California, Berkeley), except for the ones newly created in this study. *D. melanogaster* strains were maintained at two different locations with different settings. At UC Berkeley, flies were maintained at 24°C on a 12L:12D cycle and reared on molasses-cornmeal media from UC Berkeley Fly Food Facility. At National Institute of Physiological Sciences (NIPS), flies were maintained at 25°C on a 12L:12D cycle and reared on in-house glucose-cornmeal media (Sato et al. 2023). Flies at NIPS were used for behavioral assay with ectopic TRPA1 expression (Figure 5). All other experiments using *D. melanogaster* were performed with the strains at UC Berkeley.

Behavioral assay (Wild-type). PER is a common behavior assay in *Drosophila* to measure feeding preference to a given chemical by monitoring the frequency of proboscis extension after the presentation of test chemicals (Shiraiwa and Carlson 2007). We first conducted PER assay to characterize species-specific preference towards allyl isothiocyanates (AITC). Our protocol for PER assay was based on (Kang et al. 2010) with several modifications.

Adult flies were collected from their larval media soon after the emergence and transferred to plastic vials containing a cotton ball with 10% honey water (pure organic honey purchased at Trader Joe's, CA) to account for larval food differences. We did not separate male and female flies during this period, thus we assume that all female flies were already mated at the time of experiments. 2-9 day old flies were starved for 24 hours in a foodless humidified vial prior to the assay. Flies were then anesthetized with CO_2, mounted on a glass slide dorsal side down using nail polish, and allowed to recover in a humidified chamber for at least 2 hours. Flies that did not show active leg movement after the 2-hour recovery period were removed from the assay. During the PER assay, all flies were first satiated with water, and each fly was offered a single type of tastant (i.e., 300 mM sucrose solution or its mixture with a given concentration of AITC) by touching their forelegs with test chemicals as a small droplet from a P200

947 pipette tip. We picked AITC as a representative ITC for this and subsequent
948 experiments, because it is the most commonly used ITC in previous laboratory-based
949 studies using *Drosophila*. Each presentation continued up to 10 seconds, and the
950 response of a fly to the tastant within the 10-second window was scored based on our
951 criteria: 1 pt - extended proboscis and maintained drinking the droplet >2 seconds; 0.5
952 pt - extended proboscis but failed to maintain contact to the droplet, or only showed
953 brief contact; 0 pt - did not show proboscis extension and failed to contact the droplet.
954 Feeding droplet was immediately withdrawn when a fly continued PER for 3 seconds to
955 minimize satiety. Presentation was repeated five times per fly (with a 5-10 minute
956 interval between presentations), such that each fly accumulated a total score in a range
957 between 0 to 5. We performed PER assay at four different AITC concentrations (i.e., 0,
958 2, 5, 10 mM AITC in a 300 mM sucrose solution), assuming the biological ITC
959 concentrations for the Brassicales plants were somewhere between 1 mM to 5 mM. We
960 tested n= 19-34 individual flies at each combination of species, sex, and AITC
961 concentration (see Supplementary Table). All experiments were performed at zeitgeber
962 time (ZT) 7-10.

963 To visually highlight the degree of feeding inhibition, average PER scores at each
964 treatment was normalized to that of 0 mM AITC within species, in which the PER score
965 closer to 0 indicated the stronger feeding inhibition by AITC (Figure 1B and S1). We did
966 not present error bars in the figures because of this normalization. The difference in
967 feeding response across the AITC dosage series was tested within each species/sex
968 combination using pairwise Wilcoxon rank-sum test with Benjamini-Hochberg correction
969 based on pre-normalized individual PER scores. See Supplementary Tables for the raw
970 data and the associations between original and normalized PER scores.

971

972 **Generation of transgenic flies.** We performed genetic rescue experiments in *TrpA1*
973 null-mutant *D. melanogaster* lines to test whether the ectopic expression of *Scaptomyza*
974 TRPA1 sufficiently recapitulates the behavioral variation of wild-type species. We
975 focused our efforts on TRPA1-CL(C) isoform because it is the only predominantly
976 expressed isoform across the three species (Figure 3B). We first digested the fly
977 transgenesis vector pUAST::attB (Bischof et al. 2007) using NotI-HF and EcoRI-HF
978 restriction enzymes (New England Biolab). Three *TrpA1* isoforms (*SfTrpA1-CL*,
979 *SpTrpA1-CL*, and *DmTrpA1-C*) were subcloned into pUAST::attB using NEBuilder HiFi
980 DNA Assembly Master Mix (New England Biolab). These *UAS-TrpA1* cassettes were
981 inserted into *D. melanogaster* genome targeting at attP40 site on chromosome 2 using
982 PhiC31 integrase. Transgenesis of *D. melanogaster* embryos and the initial
983 transformant screening were performed at Genetivision (Huston, TX, USA), which
984 successfully produced independent *UAS-TrpA1* lines for each *TrpA1* isoform. Other
985 mutant strains were obtained from Bloomington *Drosophila* Stock Center (#28801:
986 *pGr66a-GAL4*;*Gr93a*^{3}, #26504: *w**;*TrpA1*^{1}, #7198: *w**;*CyO/Krlf-1*;*TM3,Ser1/D*^{1}). All

987 mutant lines were initially backcrossed to *w*^{1118} for five generations to homogenize their
988 genetic background. *pGr66a-GAL4* (after omitting the *Gr93a*^{3} allele) and all *UAS-TrpA1*
989 lines were then crossed to *TrpA1*^{1} (= *TrpA1* null-mutant) lines so all flies became null
990 mutants of the endogenous *TrpA1* allele (Figure S14). Each *UAS-TrpA1*;*TrpA1*^{1} line was
991 then crossed either to *pGr66a-GAL4*;*TrpA1*^{1} line (test genotype) or to *+/+*;*TrpA1*^{1} line
992 (control genotype) to obtain the genotypes we used in experiments.
993
994 **Behavioral assay (Transgenic lines).** Procedures of the PER assay for transgenic
995 flies were identical to those for wild-type flies except for these modifications: (1) Adult
996 flies were collected soon after the emergence and kept on fresh media until the 24-hour
997 starvation period. (2) 3-6 day old female flies were used for the assay (assuming all flies
998 were mated by this period). (3) After the starvation period, individual flies were
999 transferred into P200 plastic tips (without anesthesia) such that only the head and
1000 forelegs were exposed and allowed to access tastants. As test substances, three
1001 concentrations (0, 5, 10 mM) of N-methylmaleimide (NMM) were prepared in 100 mM
1002 sucrose solution containing 0.5% DMSO. We switched from AITC that could interfere
1003 with the endogenous olfactory pathway of flies (Matsunaga et al. 2025), and instead
1004 used another TRPA1 activator, NMM, such that we can evaluate the effect of ectopic
1005 TRPA1 expression on gustatory behavior. (4) Each fly was tested with a single tastant
1006 five times, in which each presentation lasted up to 5 seconds. All assays were
1007 performed at ZT 6.5-9.5.
1008 PER scores were calculated in the same criteria as those in wild-type PER, and
1009 eventually normalized to 0 mM NMM within genotype in a range between 0 to 1.
1010 Differences in the distribution of total PER scores were statistically tested within
1011 genotypes using pairwise Wilcoxon rank-sum test with Benjamini-Hochberg correction
1012 based on pre-normalized individual PER scores. To highlight the contribution of ectopic
1013 TRPA1 expression, we further took the ratio of average PER scores between a test
1014 genotype (*Gr66a>TrpA1*;*TrpA1*^{1}) and a control genotype (*UAS-TrpA1/+*;*TrpA1*^{1}) for each
1015 TRPA1 channel expressed, and plotted the dose-responses as line graphs (Figure 5C).
1016 See Supplementary Tables for the raw data and the associations between original and
1017 normalized PER scores.
1018
1019 **Starvation tolerance assay.** Adult flies were collected upon emergence and reared on
1020 10% honey water. 8-10 flies (of 2-5 days old) of each species/sex were grouped and
1021 transferred to a plastic vial containing 1% agarose, and incubated under a laboratory
1022 condition (20-21 °C, 60% humidity, 12:12 L:D cycle). We then monitored the number of
1023 dead/live flies every 12 hours until all individuals were dead. 5-6 replicates for each
1024 species/sex group were tested. Survival rates differences between species were
1025 analyzed for each sex by pairwise log-rank test using survminer package v0.4.9
1026 (Kassambara et al. 2017) in R v4.2.1.

1027

1028 **RNA extraction and RNA-sequencing.** Adult females of *S. flava* and *S. pallida* right
1029 after the eclosion were collected from the original vials and transferred to humidified
1030 vials containing 10% honey water for up to 3 days. Labella and tarsi were
1031 hand-dissected using razors and forceps while the flies were anesthetized by CO_2.
1032 Dissected tissues were then collected in LB+TGA lysis buffer from Reliaprep RNA
1033 Tissue Miniprep System (Promega, USA) and disrupted using Biomasher Standard
1034 homogenizer (Takara Bio Inc., USA) in a dry ice ethanol bath. Approximate numbers of
1035 individuals pooled for a single replicate were 100-120 for labella and 70-75 for tarsi
1036 (forelegs, midlegs, and hindlegs were pooled). We prepared three biological replicates
1037 for each combination of species and tissue. Sample lysates were stored in -80 °C
1038 freezer until subsequent RNA extraction.

1039 Total RNA were extracted from the lysates using ReliaPrep RNA Tissue Miniprep
1040 System (Promega) according to the manufacturer's protocol, and quantified using Qubit
1041 RNA High Sensitivity kit (Thermo Fisher Scientific). Extracted RNA samples were
1042 subsequently processed into cDNA libraries using KAPA RNA HyperPrep Kit (Roche
1043 Sequencing) according to the manufacturer's protocol with a few modifications, such as
1044 the use of in-house indexing adapters developed by the Functional Genomics
1045 Laboratory (FGL), a QB3-Berkeley Core Research Facility at UC Berkeley.
1046 Approximately 300 ng total RNA for labellar samples and 100 ng for tarsal samples
1047 were used as a starting material per library. Fragment lengths of cDNA libraries were
1048 quantified with Bioanalyzer High sensitivity DNA kit (Agilent Technologies, USA) and
1049 sequenced on NovaSeq 6000 platforms (Illumina, USA) for 150 bp paired-end reads at
1050 Genome Sequencing Laboratory (GSL) at UC Berkeley. Raw RNA-seq reads were
1051 deposited to NCBI SRA database under BioProject accession number PRJNA779814.

1052

1053 **Differential gene expression analysis.** We conducted differential gene expression
1054 (DGE) analyses to compare and characterize the expression levels of *TrpA1* across
1055 species. We filtered raw RNA-seq reads using Fastp v0.21.0 (Chen et al. 2018) and
1056 mapped the clean reads on reference genomes for *S. flava (Peláez et al. 2023)* and *S.*
1057 *pallida (Kim et al. 2021)* using STAR v2.7.1a (Dobin et al. 2013) to generate BAM files.
1058 We also downloaded labellar and tarsal RNA-sequencing datasets of *D. melanogaster*
1059 female (Dweck et al. 2021; Wang et al. 2022) and mapped them onto *D. melanogaster*
1060 reference genome (BDGP6.46) in the same manner. Since *D. melanogaster* short reads
1061 were 75 bp long, we created another set of BAM files for *S. flava* by trimming the reads
1062 into 75 bp using Trim Galore v0.6.6 for the expression analysis between *D.*
1063 *melanogaster* and *S. flava*, to minimize potential biases due to read length differences
1064 (Chhangawala et al. 2015). BAM files were subsequently converted into count data
1065 using HTseq v0.9.1 (Anders et al. 2015).

1066 We next performed reciprocal BLASTN searches using the whole set of protein
1067 coding sequences of *S. flava* and *S. pallida* to identify 1-to-1 orthologous relationships
1068 between species. We screened gene pairs by bitscores and removed redundant genes
1069 using manual Python scripts, resulting in 10,439 orthologous gene pairs between *S.*
1070 *flava* and *S. pallida*. Similar procedures yielded 9,563 orthologous gene pairs between
1071 *S. flava* and *D. melanogaster*. Principal component analysis (PCA) was conducted on
1072 8,920 orthologous genes to visualize similarities among samples using prcomp package
1073 in R v4.2.1. Cross-species DGE analysis were performed using DESeq2 v1.36.0 (Love
1074 et al. 2014) with ashr for Log Fold Shrinkage (Stephens 2017). Because of the high
1075 false-positive rates intrinsic to cross-species analyses, we applied a strict cutoff
1076 (adjusted p-value < 0.001) to identify differentially expressed genes between species.
1077 We calculated TPM (transcripts per million reads) of the *TrpA1* gene based on the count
1078 data and gene lengths for each species.
1079
1080 **Fluorescent *in situ* hybridization.** We conducted RNA FISH to examine the types of
1081 gustatory neurons expressing *TrpA1* in the fly labellum. HCR (hybridization chain
1082 reaction) RNA FISH kit was ordered from Molecular Instruments (CA, USA) (Choi et al.
1083 2018). Custom mRNA probes for *D. melanogaster* and *S. flava TrpA1,* as well as *Gr66a*
1084 as a marker for bitter-sensing neurons, were designed and produced at Molecular
1085 Instruments (CA, USA). *TrpA1* probes targeted Exons 5-11 so they bind to all splicing
1086 isoforms equally. Female *D. melanogaster* and *S. flava* between 3-10 days old were
1087 anesthetized with CO_2. Their mouthparts were hand-dissected with fine forceps and
1088 fixed in a 2 mL fixative solution (4% paraformaldehyde in 1X PBS, with 0.1% Triton
1089 X-100) at 4 °C on a nutator for 24 hours. Following the fixation, samples were washed
1090 twice in 2 mL 1X PBS + 3% Triton X-100, once in 2 mL 1X PBT (i.e., PBS + 0.1% Triton
1091 X-100), and four times in 1 mL 1X PBT. Hybridization and amplification steps were
1092 mostly identical to the manufacturer's protocol for *D. melanogaster* embryos, except for
1093 the higher probe/hairpin concentrations suggested in (Bontonou et al. 2024): probe
1094 solutions were created by adding 5 µL each of experimental (*TrpA1*) and control (*Gr66a*)
1095 probes to 300 µL probe hybridization buffer. Likewise, hairpin solutions were prepared
1096 by adding 10 µL of each 3 µM hairpin stock to 300 µL amplification solution.
1097 Samples were imaged with a Zeiss LSM 880 microscope using an Airyscan
1098 detector and a 63x/1.4NA oil immersion objective. *Gr66a* and *TrpA1* mRNAs were
1099 visualized using the 488 nm (3% power) and 561 nm (2% power) excitation lasers,
1100 respectively. Z-stacks were acquired with 944 x 944 pixel image resolution, with a pixel
1101 size of 0.07 µm and 0.2 µm step size. After acquisition in Airyscan Fast mode, raw
1102 images were deconvolved using the Zen Black software. Airyscan-processed images
1103 were subsequently analyzed using Fiji (ImageJ).
1104

1105 **Detection of *TrpA1* splicing variants and orthologues.** To predict mRNA structures
1106 of *Scaptomyza TrpA1* splice variants, we first conducted *de novo* assembly of
1107 aforementioned RNA-seq short reads using Trinity v2.5.1 (Grabherr et al. 2011), and
1108 subsequently ran TBLASTN searches (v2.10.1) against the assembled contigs of *S.*
1109 *flava* and *S. pallida* using *D. melanogaster* TRPA1-C protein sequence as a query.
1110 Exonic structures of *S. flava* and *S. pallida TrpA1s* were manually inspected from
1111 sequence alignments using MAFFT v7.273 (Katoh and Standley 2013) and
1112 aforementioned BAM flies using IGV v2.9.4 (Thorvaldsdóttir et al. 2013) after the
1113 BLAST search against their respective reference genomes. Presence of a certain *TrpA1*
1114 isoforms was further confirmed by PCR-based subcloning using labellar and tarsal
1115 cDNA samples of the two *Scaptomyza* species.

1116 *TrpA1* orthologues from other species were obtained from the NCBI database or
1117 detected by TBLASTN searches against reference genomes using *S. flava* TRPA1-CL
1118 as a query. Putative exons at the N-terminal region of *D. melanogaster*, *D. mojavensis*,
1119 *D. grimshawi*, *S. hsui*, *S. graminum, and S. montana TrpA1s* were also identified based
1120 on BLAST searches and manual inspection of their genomic sequences. For *D.*
1121 *melanogaster* and *D. mojavensis*, NCBI-deposited RNA-seq data were mapped on their
1122 genomes using STAR v2.7.1a (Dobin et al. 2013) and referred as additional evidence
1123 for the transcription of *TrpA1* splicing variants.

1124

1125 **Amplicon sequencing and analyses of isoform compositions.** We next aimed to
1126 quantify the proportions of expressed *TrpA1* isoforms in fly labella and tarsi to
1127 investigate whether the isoform compositions are associated with the dietary adaptation
1128 of the flies. Due to the nature of *Scaptomyza/Drosophila TrpA1* isoforms where exons
1129 defining isoform types are distantly located (i.e., ~2 kb on mRNA, Figure 3A), common
1130 gene expression analyses such as short-read sequencing or quantitative PCR do not
1131 accurately capture the proportions of *TrpA1* splicing variants. Therefore, we employed
1132 amplicon sequencing targeting the entire *TrpA1* cDNA using a long-read sequencer
1133 MinION (Oxford Nanopore Technologies), assuming the ratio of *TrpA1* isoforms was still
1134 conserved after PCR amplification (Figure S7).

1135 Our experimental procedures modified those introduced in (Clark et al. 2020; Hall
1136 et al. 2021). Total RNA was extracted from independent groups of fly labella or tarsi
1137 (forelegs, midlegs, and hindlegs were pooled), wherein each replicate contained roughly
1138 40-50 individuals. 100 ng labellar total RNA or 50 ng tarsal total RNA were transcribed
1139 into cDNA using SuperScript IV (Invitrogen, USA). These cDNAs were later used as
1140 templates for the first-round PCR for *TrpA1* transcripts using Phusion High-Fidelity DNA
1141 polymerase (New England Biolab). PCR primers were designed for the first exon (i.e.,
1142 Exon L; usually considered a 5'UTR in *Drosophila TrpA1*) and the last exons (i.e., Exon
1143 18) such that the entire pool of *TrpA1* isoforms can be amplified in a single reaction
1144 (Figure 3A, Figure S7). Furthermore, the primers were concatenated to common

1145 “adapter” sequences acting as annealing sites for barcoding primers in the
1146 second-round barcoding PCR (Figure S7). Successful *TrpA1* amplicons were isolated
1147 from 1% agarose gel after electrophoresis and purified using Monarch DNA gel
1148 extraction kit (New England Biolab). We were not able to recover *TrpA1* amplicons from
1149 *D. melanogaster* tarsal cDNA, possibly because of its low expression levels (Figure 2F),
1150 thus it was omitted from the downstream analysis. 40 ng *TrpA1* amplicons were then
1151 used as templates for the second-round barcoding PCR using LongAmp Taq 2X Master
1152 Mix (New England Biolab) and PCR Barcoding Expansion (EXP-PBC001, Oxford
1153 Nanopore Technologies). Barcoded *TrpA1* fragments were cleaned with QIAquick PCR
1154 Purification Kit (Qiagen) and quantified with Qubit dsDNA BR Assay Kit (Thermo Fisher
1155 Scientific). Subsequently, multiple *TrpA1* amplicons were pooled together in a single
1156 tube for size selection using X0.6 SPRIselect magnetic beads (Beckman Coulter, USA).
1157 Selected fragments were used for library preparation using Ligation Sequencing Kit
1158 (SQK-LSK109, Oxford Nanopore Technologies). Libraries were sequenced on Flongle
1159 Flow Cell (R9.4.1; Oxford Nanopore Technologies) with MinION Mk1B sequencer
1160 (Oxford Nanopore Technologies) and MinKNOW platform v22.12.7. Basecalling was
1161 concurrently performed with sequencing using Guppy v6.4.6.

1162 After obtaining sequencing output as FASTQ files, we performed BLASTN
1163 searches against the outputs using pre-annotated *TrpA1* isoform sequences as queries
1164 to figure out the isoform type of each single read. To take into account the high error
1165 rates intrinsic to ONT long-read sequencers, we used in-house Python scripts to filter
1166 out the reads where the lengths were outside the range between 3.8 and 4.5 kb or the
1167 sequence similarity to the best hit gene model was less than 85%. Passed reads were
1168 categorized as their best-hit *TrpA1* isoform type, and the proportions of the isoforms
1169 were calculated. The relative proportions of each *TrpA1* isoform type were fitted into a
1170 generalized linear model (GLM) assuming Gaussian distribution using R v4.2.1, and the
1171 difference between groups were tested with Tukey’s post hoc HSD test with
1172 Benjamini-Hochberg correction.

1173

1174 **Structural analysis.** We predicted structures of *S. flava* and *S. pallida* TRPA1s using
1175 the AlphaFold Server (Abramson et al. 2024) based on their amino acid sequences.
1176 Putative structural changes by amino acid substitutions were investigated by simply
1177 editing the residues on input sequences.

1178

1179 **Oocyte electrophysiology.** We performed two-electrode voltage clamp (TEVC)
1180 recordings using *Xenopus laevis* oocytes to characterize activity and sensitivity of
1181 detected TRPA1 isoforms. A *Xenopus* expression vector pOX(+) (Dowland et al. 2000)
1182 was first digested by restriction enzymes AflII and NotI-HF (New England Biolab). Nine
1183 *Scaptomyza*/*Drosophila TrpA1* isoform CDSs were then subcloned into pOX(+) using
1184 NEBuilder HiFi DNA Assembly Master Mix (New England Biolab). Original *TrpA1*

1185 sequences were obtained from various sources (see Key Resource Table). cDNA
1186 synthesis was conducted with 40-80ng starting total RNA using Superscript IV
1187 (Invitrogen). pOX(+)-*TrpA1* constructs were linearized with restriction enzyme RsrII
1188 (New England Biolab) and used as templates for cRNA (complementary RNA) synthesis
1189 using mMessage mMachine SP6 Transcription kit (Thermo Fisher Scientific). All TRPA1
1190 cRNAs were diluted to 50 ng/μL concentration.

1191 Oocytes were collected from adult *Xenopus laevis* and processed with
1192 Collagenase A (Roche) to remove follicular membranes. 50 nL of diluted cRNA (50
1193 ng/μL) was injected into each single oocyte 1-2 days after the egg retrieval.
1194 Two-electrode voltage clamp (TEVC) recordings were performed 2-3 days post injection
1195 using OC-725C amplifier (Warner Instruments, USA) with a 1 kHz low-pass filter and
1196 digitized at 5 kHz Digidata 1440 (Molecular Devices, USA). Oocytes were positioned in
1197 a bath-filled oocyte chamber and clamped at -60 mV during the recordings. ND96 (96
1198 mM NaCl, 2 mM KCl, 1.8 mM $CaCl_2$, 1 mM $MgCl_2$, and 5 mM HEPES; pH 7.4) was used
1199 as the bath solution during the entire recordings. Bath temperature was monitored using
1200 a thermistor in an oocyte chamber and TC-344B dual channel temperature controller
1201 (Warner Instruments). AITC for chemical stimulation was first prepared in DMSO at
1202 0.001, 0.01, 0.03, 0.1, 0.3, 1, and 3 M concentrations, each of which was further diluted
1203 1,000-fold with bath solution prior to the recording. Heat stimulation was conducted by
1204 perfusing heated bath solution to the chamber. Taking advantage of the polymodal
1205 nature of fly TRPA1, we stimulated the channels twice in the course of a single
1206 recording. Oocytes were first heated (>40 °C) for 30 seconds, washed for 120 seconds,
1207 and then challenged with a single dosage of AITC for 90 seconds. This design allowed
1208 us to normalize a peak amplitude of an AITC-evoked raw current (I_{AITC}) by the amplitude
1209 of heat-evoked raw current (I_{Heat}). When the current response did not saturate within the
1210 90-second AITC stimulation, I_{AITC} was considered as the amplitude at the end of the
1211 90-second window. Recordings were performed at a series of concentrations ranging
1212 from 0.001 mM to 3 mM AITC. Raw current values were retrieved using Clampfit
1213 v11.2.0.61 (Molecular Devices). Normalized current value (I_{AITC}/I_{Heat}) from each recording
1214 was used to estimate dose-response relationships and EC_{50} for each TRPA1 isoform
1215 using R package drc v3.0-1 (Ritz et al. 2015) under the LL.3 function. To investigate
1216 potential biases due to the difference of heat activation, I_{Heat} from all recordings were
1217 merged for each canonical isoform type (i.e., TRPA1-CL or TRPA1-DL) and analyzed
1218 between species using Kruskal-Wallis test, followed by Conover's post hoc test with
1219 Benjamini-Hochberg correction using R v4.2.1.

1220 TEVC recordings with the co-expression of multiple TRPA1 isoforms were
1221 performed in the same manner, except that diluted 50 ng/μL cRNAs were mixed in a
1222 given ratio prior to the microinjection. Expression ratios of *TrpA1-CL* to *TrpA1-DL* mRNA
1223 in four tissues (i.e., *S. flava* female labella, *S. pallida* labella, *S. flava* female tarsi, *S.*
1224 *pallida* tarsi) were determined by taking an average of three biological replicates of

amplicon read count data (Figure 3B) and approximating it to the closest integer ratio. Note that we used raw AITC-evoked currents (I_{AITC}) for the analyses of inactive TRPA1 isoforms (i.e., SfTRPA1-CS, SfTRPA1-DS, SpTRPA1-EL) because their small heat-evoked currents (I_{Heat}) prevented accurate normalization. Differences in labellar or tarsal mRNA mixtures between species (Figure 6C and 6D) were tested by Student's t-test or Welch's t-test depending on the fulfillment of parametric assumptions. Differences among the isoform mixtures within a single species (i.e., canonical/inactive isoform mixtures (Fig. 7D and 7E) and single isoforms vs. labellar/tarsal mixtures (Figure 6A and 6B)) were analyzed using one-way ANOVA followed by Tukey's post hoc test, or Kruskal-Wallis test followed by Conover's post-hoc test with Benjamini-Hochberg correction, also depending on the fulfillment of parametric assumptions. All statistical analyses were run on R v4.2.1.

ACKNOWLEDGEMENTS

We thank Carolina Reisenman, Kirsten Verster, Rebecca Tarnopol, Marianthi Karageorgi, Lydia Smith, Rebecca Duncan, Susan Bernstein, Jessica Aguilar, Benjamin Goldman-Huertas, Samridhi Chaturvedi, Moe Bakhtiari, Gary Karpen, Meghan Laturney, Diana Bautista, Oscar Arenas, Juliana Valencia Lesmes, Rebecca Tarvin, Kristin Scott (University of California, Berkeley), Shoma Sato (National Institute of Physiological Sciences, Japan), Lucia Prieto-Godino, Juan Lugo Ramos (Francis Crick Institute), Gwénaëlle Bontonou, Roman Arguello (University of Lausanne), Ryoya Tanaka, Yuki Ishikawa (Nagoya University), Hiroki Takahashi (National Institute of Basic Biology, Japan), KyeongJin Kang (Korea Brain Research Institute), and Paul Garrity (Brandeis University) for their experimental support and helpful discussions. We thank Marco Gallio and Alessia Para (Northwestern University) for sharing with us the dTRPA1-D construct. We thank David Julius and John Lin-King (University of California, San Francisco) for their early support for this project and in facilitating pilot experiments. This project was primarily supported by funding from the National Institute of General Medical Sciences of the National Institutes of Health Grant (award no. R35GM119816) to N.K.W. S.R. was supported by the NIH Grant (award no. R35GM139653) to Gary H. Karpen. S.C.G. was supported by the NIH Grant (award no. R35GM151194) awarded to S.C.G.

AUTHOR CONTRIBUTIONS

H.C.S., S.C.G., and N.K.W. conceived the project. H.C.S., S.S., and N.K.W. designed the experiments with major contributions from D.H. (on *TrpA1* amplicon sequencing), S.R. (on HCR RNA-FISH), and T.S. (on transgenic fly crossing and subsequent PER assay). H.C.S. performed all behavioral experiments, bioinformatics, and statistical analyses. H.C.S., J.N.P., T.M., and A.S.T. performed fly tissue dissection, RNA extraction, and molecular biology, and K.M.T. and A.T. supported the experiments. H.C.S. and C.T.S. performed oocyte electrophysiology and data analyses under the supervision of S.S. and M.T. S.R. performed microscopy. H.C.S. and N.K.W. drafted and revised the manuscript, and all authors provided comments and contributed to editing the manuscript.

DECLARATION OF INTERESTS

The authors declare no competing interests.

REFERENCES

Abramson J, Adler J, Dunger J, Evans R, Green T, Pritzel A, Ronneberger O, Willmore L, Ballard AJ, Bambrick J, et al. 2024. Accurate structure prediction of biomolecular interactions with AlphaFold 3. *Nature* 630:493–500.

Aguilar JM, Gloss AD, Suzuki HC, Verster KI, Singhal M, Hoff J, Grebenok R, Nabity PD, Behmer ST, Whiteman NK. 2024. Insights into the evolution of herbivory from a leaf-mining fly. *Ecosphere* 15:e4764.

Akashi HD, Saito S, Cádiz Díaz A, Makino T, Tominaga M, Kawata M. 2018. Comparisons of behavioural and TRPA1 heat sensitivities in three sympatric Cuban Anolis lizards. *Mol. Ecol.* 27:2234–2242.

Álvarez-Ocaña R, Shahandeh MP, Ray V, Auer TO, Gompel N, Benton R. 2023. Odor-regulated oviposition behavior in an ecological specialist. *Nat. Commun.* 14:3041.

Anders S, Pyl PT, Huber W. 2015. HTSeq--a Python framework to work with high-throughput sequencing data. *Bioinformatics* 31:166–169.

Arenas OM, Zaharieva EE, Para A, Vásquez-Doorman C, Petersen CP, Gallio M. 2017. Activation of planarian TRPA1 by reactive oxygen species reveals a conserved mechanism for animal nociception. *Nat. Neurosci.* 20:1686–1693.

Auer TO, Khallaf MA, Silbering AF, Zappia G, Ellis K, Álvarez-Ocaña R, Arguello JR, Hansson BS, Jefferis GSXE, Caron SJC, et al. 2020. Olfactory receptor and circuit evolution promote host specialization. *Nature* 579:402–408.

Bendesky A, Bargmann CI. 2011. Genetic contributions to behavioural diversity at the gene–environment interface. *Nat. Rev. Genet.* 12:809–820.

Bischof J, Maeda RK, Hediger M, Karch F, Basler K. 2007. An optimized transgenesis system for Drosophila using germ-line-specific phiC31 integrases. *Proc. Natl. Acad. Sci. U. S. A.* 104:3312–3317.

Bontonou G, Saint-Leandre B, Kafle T, Baticle T, Hassan A, Sánchez-Alcañiz JA, Arguello JR. 2024. Evolution of chemosensory tissues and cells across ecologically diverse Drosophilids. *Nat. Commun.* 15:1047.

Brand P, Hinojosa-Díaz IA, Ayala R, Daigle M, Yurrita Obiols CL, Eltz T, Ramírez SR. 2020. The evolution of sexual signaling is linked to odorant receptor tuning in perfume-collecting orchid bees. *Nat. Commun.* 11:244.

Capek M, Arenas OM, Alpert MH, Zaharieva EE, Méndez-González ID, Simões JM, Gil H, Acosta A, Su Y, Para A, et al. 2025. Evolution of temperature preference in flies of the genus Drosophila. *Nature* [Internet]. Available from:

http://dx.doi.org/10.1038/s41586-025-08682-z

Chen S, Zhou Y, Chen Y, Gu J. 2018. fastp: an ultra-fast all-in-one FASTQ preprocessor. *Bioinformatics* 34:i884–i890.

Chhangawala S, Rudy G, Mason CE, Rosenfeld JA. 2015. The impact of read length on quantification of differentially expressed genes and splice junction detection. *Genome Biol.* 16:1–10.

Choi HMT, Schwarzkopf M, Fornace ME, Acharya A, Artavanis G, Stegmaier J, Cunha A, Pierce NA. 2018. Third-generation in situ hybridization chain reaction: multiplexed, quantitative, sensitive, versatile, robust. *Development* 145:dev165753.

Clark MB, Wrzesinski T, Garcia AB, Hall NAL, Kleinman JE, Hyde T, Weinberger DR, Harrison PJ, Haerty W, Tunbridge EM. 2020. Long-read sequencing reveals the complex splicing profile of the psychiatric risk gene CACNA1C in human brain. *Mol. Psychiatry* 25:37–47.

Cordero-Morales JF, Gracheva EO, Julius D. 2011. Cytoplasmic ankyrin repeats of transient receptor potential A1 (TRPA1) dictate sensitivity to thermal and chemical stimuli. *Proceedings of the National Academy of Sciences* 108:E1184–E1191.

Diaz F, Allan CW, Matzkin LM. 2018. Positive selection at sites of chemosensory genes is associated with the recent divergence and local ecological adaptation in cactophilic Drosophila. *BMC Evol. Biol.* 18:144.

Dobin A, Davis CA, Schlesinger F, Drenkow J, Zaleski C, Jha S, Batut P, Chaisson M, Gingeras TR. 2013. STAR: ultrafast universal RNA-seq aligner. *Bioinformatics* 29:15–21.

Dowland LK, Luyckx VA, Enck AH, Leclercq B, Yu AS. 2000. Molecular cloning and characterization of an intracellular chloride channel in the proximal tubule cell line, LLC-PK1. *J. Biol. Chem.* 275:37765–37773.

Duckworth RA. 2009. The role of behavior in evolution: a search for mechanism. *Evol. Ecol.* 23:513–531.

Du EJ, Lee M, Kim SY, Park SH, Ohk H-J, Kang K. 2024. Linkage of alternative exon assembly in Drosophila TrpA1 transcripts. *Mol. Cells* 47:100110.

Dweck HK, Talross GJ, Wang W, Carlson JR. 2021. Evolutionary shifts in taste coding in the fruit pest Drosophila suzukii. *Elife* [Internet] 10. Available from: http://dx.doi.org/10.7554/eLife.64317

Edger PP, Heidel-Fischer HM, Bekaert M, Rota J, Glöckner G, Platts AE, Heckel DG, Der JP, Wafula EK, Tang M, et al. 2015. The butterfly plant arms-race escalated by gene and genome duplications. *Proceedings of the National Academy of Sciences* 112:8362–8366.

Eigenbrod O, Debus KY, Reznick J, Bennet NC, Sánchez-Carranza O, Omerbasic D, Hart DW, Barker AJ, Zhong W, Lutermann H, et al. 2019. Rapid molecular evolution of pain insensitivity in multiple African rodents. *Science* 859:852–859.

Finch S. 1978. VOLATILE PLANT CHEMICALS AND THEIR EFFECT ON HOST PLANT FINDING BY THE CABBAGE ROOT FLY (DELIA BRASSICAE). *Entomol. Exp. Appl.* 24:150–159.

Gloss AD, Dittrich ACN, Lapoint RT, Huertas BG, Verster KI, Pelaez JL, Nelson ADL, Aguilar J, Armstrong E, Charboneau JLM, et al. 2019. Evolution of herbivory remodels a Drosophila genome. *bioRxiv*:767160.

Gloss AD, Vassão DG, Hailey AL, Nelson Dittrich AC, Schramm K, Reichelt M, Rast TJ, Weichsel A, Cravens MG, Gershenzon J, et al. 2014. Evolution in an ancient detoxification pathway is coupled with a transition to herbivory in the drosophilidae. *Mol. Biol. Evol.* 31:2441–2456.

Goldman-Huertas B, Mitchell RF, Lapoint RT, Faucher CP, Hildebrand JG, Whiteman NK. 2015. Evolution of herbivory in Drosophilidae linked to loss of behaviors, antennal responses, odorant receptors, and ancestral diet. *Proceedings of the National Academy of Sciences* 112:3026–3031.

Grabherr MG, Haas BJ, Yassour M, Levin JZ, Thompson DA, Amit I, Adiconis X, Fan L, Raychowdhury R, Zeng Q, et al. 2011. Trinity: reconstructing a full-length transcriptome without a genome from RNA-Seq data. *Nat. Biotechnol.* 29:644–652.

Gracheva EO, Cordero-Morales JF, González-Carcacía JA, Ingolia NT, Manno C, Aranguren CI, Weissman JS, Julius D. 2011. Ganglion-specific splicing of TRPV1 underlies infrared sensation in vampire bats. *Nature* 476:88–92.

Gracheva EO, Ingolia NT, Kelly YM, Cordero-Morales JF, Hollopeter G, Chesler AT, Sánchez EE, Perez JC, Weissman JS, Julius D. 2010. Molecular basis of infrared detection by snakes. *Nature* 464:1006–1011.

Guo L, Qiao X, Haji D, Zhou T, Liu Z, Whiteman NK, Huang J. 2023. Convergent resistance to GABA receptor neurotoxins through plant–insect coevolution. *Nature Ecology & Evolution*:1–13.

Gu P, Gong J, Shang Y, Wang F, Ruppell KT, Ma Z, Sheehan AE, Freeman MR, Xiang Y. 2019. Polymodal Nociception in Drosophila Requires Alternative Splicing of TrpA1. *Curr. Biol.* 29:3961–3973.e6.

Gu P, Wang F, Shang Y, Liu J, Gong J, Xie W, Han J, Xiang Y. 2022. Nociception and hypersensitivity involve distinct neurons and molecular transducers in Drosophila. *Proc. Natl. Acad. Sci. U. S. A.* 119:e2113645119.

Hall NAL, Husain SM, Lee H, Tunbridge EM. 2021. Long read transcript profiling of ion channel splice isoforms. *Methods Enzymol.* 654:345–364.

1382 Himmel NJ, Cox DN. 2020. Transient receptor potential channels: current perspectives
1383 on evolution, structure, function and nomenclature. *Proc. Biol. Sci.* 287:20201309.

1384 Hinman A, Chuang H-H, Bautista DM, Julius D. 2006. TRP channel activation by
1385 reversible covalent modification. *Proc. Natl. Acad. Sci. U. S. A.* 103:19564–19568.

1386 Huang X, Renwick JAA, Sachdev-Gupta K. 1993. A chemical basis for deifferential
1387 acceptance of Erysimum cheiranthoides by two Pieris species. *J. Chem. Ecol.*
1388 19:195–210.

1389 Huang X, Renwick JAA, Sachdev-Gupta K. 1993. Oviposition stimulants and deterrents
1390 regulating differential acceptance of Iberis amara by Pieris rapae and P. napi
1391 oleracea. *J. Chem. Ecol.* 19:1645–1663.

1392 Inagaki HK, Panse KM, Anderson DJ. 2014. Independent, reciprocal neuromodulatory
1393 control of sweet and bitter taste sensitivity during starvation in Drosophila. *Neuron*
1394 84:806–820.

1395 Jordt SE, Bautista DM, Chuang HH, McKemy DD, Zygmunt PM, Högestätt ED, Meng
1396 ID, Julius D. 2004. Mustard oils and cannabinoids excite sensory nerve fibres
1397 through the TRP channel ANKTM1. *Nature* 427:260–265.

1398 Kang K, Panzano VC, Chang EC, Ni L, Dainis AM, Jenkins AM, Regna K, Muskavitch
1399 MAT, Garrity PA. 2012. Modulation of TRPA1 thermal sensitivity enables sensory
1400 discrimination in Drosophila. *Nature* 481:76–81.

1401 Kang K, Pulver SR, Panzano VC, Chang EC, Griffith LC, Theobald DL, Garrity PA.
1402 2010. Analysis of Drosophila TRPA1 reveals an ancient origin for human chemical
1403 nociception. *Nature* 464:597–600.

1404 Karageorgi M, Bräcker LB, Lebreton S, Minervino C, Cavey M, Siju KP, Grunwald
1405 Kadow IC, Gompel N, Prud'homme B. 2017. Evolution of Multiple Sensory Systems
1406 Drives Novel Egg-Laying Behavior in the Fruit Pest Drosophila suzukii. *Curr. Biol.*
1407 27:847–853.

1408 Kassambara A, Kosinski M, Biecek P, Fabian S. 2017. Package "survminer." *Drawing*
1409 *Survival Curves using "ggplot2"(R package version 03 1)* 3.

1410 Katoh K, Standley DM. 2013. MAFFT multiple sequence alignment software version 7:
1411 Improvements in performance and usability. *Mol. Biol. Evol.* 30:772–780.

1412 Khallaf MA, Auer TO, Grabe V, Depetris-Chauvin A, Ammagarahalli B, Zhang D-D,
1413 Lavista-Llanos S, Kaftan F, Weißflog J, Matzkin LM, et al. 2020. Mate discrimination
1414 among subspecies through a conserved olfactory pathway. *Science Advances*
1415 6:eaba5279.

1416 Kim BY, Wang JR, Miller DE, Barmina O, Delaney E, Thompson A, Comeault AA,
1417 Peede D, D'Agostino ER, Pelaez J, et al. 2021. Highly contiguous assemblies of

101 drosophilid genomes. *Elife* [Internet] 10. Available from: http://dx.doi.org/10.7554/eLife.66405

Lapoint RT, O'Grady PM, Whiteman NK. 2013. Diversification and dispersal of the Hawaiian Drosophilidae: The evolution of Scaptomyza. *Mol. Phylogenet. Evol.* 69:95–108.

Lee Y, Moon SJ, Montell C. 2009. Multiple gustatory receptors required for the caffeine response in Drosophila. *Proc. Natl. Acad. Sci. U. S. A.* 106:4495–4500.

Leung NY, Thakur DP, Gurav AS, Kim SH, Di Pizio A, Niv MY, Montell C. 2020. Functions of Opsins in Drosophila Taste. *Curr. Biol.* 30:1367–1379.e6.

Lichtenstein EP, Morgan DG, Mueller CH. 1964. Insecticides in Nature:Naturally Occurring Insecticides in Cruciferous Crops. *J. Agric. Food Chem.* 12:158–161.

Li Y, Hoffmann J, Li Y, Stephano F, Bruchhaus I, Fink C, Roeder T. 2016. Octopamine controls starvation resistance, life span and metabolic traits in Drosophila. *Sci. Rep.* 6:35359.

Love MI, Huber W, Anders S. 2014. Moderated estimation of fold change and dispersion for RNA-seq data with DESeq2. *Genome Biol.* 15:550.

Macpherson LJ, Dubin AE, Evans MJ, Marr F, Schultz PG, Cravatt BF, Patapoutian A. 2007. Noxious compounds activate TRPA1 ion channels through covalent modification of cysteines. *Nature* 445:541–545.

Matsunaga AT, Reisenman CE, Goldman-Huertas B, Suzuki HC, Tadres D, Louis M, Ramírez SR, K. N. 2025. Olfactory receptors tuned to isothiocyanates in Drosophila melanogaster and their evolutionary 3 expansion in herbivorous relatives. *bioRxiv*:617316.

Matsunaga T, Reisenman CE, Goldman-Huertas B, Brand P, Miao K, Suzuki HC, Verster KI, Ramírez SR, Whiteman NK. 2022. Evolution of Olfactory Receptors Tuned to Mustard Oils in Herbivorous Drosophilidae. *Mol. Biol. Evol.* [Internet] 39. Available from: http://dx.doi.org/10.1093/molbev/msab362

McBride CS. 2007. Rapid evolution of smell and taste receptor genes during host specialization in Drosophila sechellia. *Proceedings of the National Academy of Sciences* 104:4996–5001.

McBride CS, Arguello JR. 2007. Five Drosophila genomes reveal nonneutral evolution and the signature of host specialization in the chemoreceptor superfamily. *Genetics* 177:1395–1416.

McBride CS, Baier F, Omondi AB, Spitzer SA, Lutomiah J, Sang R, Ignell R, Vosshall LB. 2014. Evolution of mosquito preference for humans linked to an odorant receptor. *Nature* 515:222–227.

Montell C. 2021. Drosophila sensory receptors—a set of molecular Swiss Army Knives. *Genetics* [Internet] 217. Available from: https://academic.oup.com/genetics/article-abstract/217/1/iyaa011/6128801

Nishida R, Ohsugi T, Kokubo S, Fukami H. 1987. Oviposition stimulants of a Citrus-feeding swallowtail butterfly, Papilio xuthus L. *Experientia* 43:342–344.

Oh SM, Jeong K, Seo JT, Moon SJ. 2021. Multisensory interactions regulate feeding behavior in Drosophila. *Proc. Natl. Acad. Sci. U. S. A.* [Internet] 118. Available from: http://dx.doi.org/10.1073/pnas.2004523118

Okamura Y, Dort H, Reichelt M, Tunström K, Wheat CW, Vogel H. 2022. Testing hypotheses of a coevolutionary key innovation reveals a complex suite of traits involved in defusing the mustard oil bomb. *Proc. Natl. Acad. Sci. U. S. A.* 119:e2208447119.

Ozaki K, Ryuda M, Yamada A, Utoguchi A, Ishimoto H, Calas D, Marion-Poll F, Tanimura T, Yoshikawa H. 2011. A gustatory receptor involved in host plant recognition for oviposition of a swallowtail butterfly. *Nat. Commun.* 2:542.

Peláez JN, Gloss AD, Goldman-Huertas B, Kim B, Lapoint RT, Pimentel-Solorio G, Verster KI, Aguilar JM, Nelson Dittrich AC, Singhal M, et al. 2023. Evolution of chemosensory and detoxification gene families across herbivorous Drosophilidae. *G3* [Internet] 13. Available from: http://dx.doi.org/10.1093/g3journal/jkad133

Peláez JN, Gloss AD, Ray JF, Chaturvedi S, Haji D, Charboneau JLM, Verster KI, Whiteman NK. 2022. Evolution and genomic basis of the plant-penetrating ovipositor: a key morphological trait in herbivorous Drosophilidae. *Proc. Biol. Sci.* 289:20221938.

Prieto-Godino LL, Rytz R, Cruchet S, Bargeton B, Abuin L, Silbering AF, Ruta V, Dal Peraro M, Benton R. 2017. Evolution of Acid-Sensing Olfactory Circuits in Drosophilids. *Neuron* 93:661–676.e6.

Ritz C, Baty F, Streibig JC, Gerhard D. 2015. Dose-Response Analysis Using R. *PLoS One* 10:e0146021.

Ryuda M, Calas-List D, Yamada A, Marion-Poll F, Yoshikawa H, Tanimura T, Ozaki K. 2013. Gustatory Sensing Mechanism Coding for Multiple Oviposition Stimulants in the Swallowtail Butterfly, Papilio Xuthus. *Journal of Neuroscience* 33:914–924.

Saito S, Saito CT, Igawa T, Takeda N, Komaki S, Ohta T, Tominaga M. 2022. Evolutionary Tuning of Transient Receptor Potential Ankyrin 1 Underlies the Variation in Heat Avoidance Behaviors among Frog Species Inhabiting Diverse Thermal Niches. *Mol. Biol. Evol.* 39:msac180.

Sato S, Magaji AM, Tominaga M, Sokabe T. 2023. Avoidance of thiazoline compound depends on multiple sensory pathways mediated by TrpA1 and ORs in Drosophila.

1491 *Front. Mol. Neurosci.* 16:1249715.

1492 Scott K. 2018. Gustatory Processing in *Drosophila melanogaster*. *Annu. Rev. Entomol.*
1493 63:15–30.

1494 Shiraiwa T. 2008. Multimodal chemosensory integration through the maxillary palp in
1495 Drosophila. *PLoS One* 3:e2191.

1496 Shiraiwa T, Carlson JR. 2007. Proboscis extension response (PER) assay in
1497 Drosophila. *J. Vis. Exp.*:193.

1498 Stephens M. 2017. False discovery rates: a new deal. *Biostatistics* 18:275–294.

1499 Talavera K, Startek JB, Alvarez-Collazo J, Boonen B, Alpizar YA, Sanchez A, Naert R,
1500 Nilius B. 2020. Mammalian Transient Receptor Potential TRPA1 Channels: From
1501 Structure to Disease. *Physiol. Rev.* 100:725–803.

1502 Thorvaldsdóttir H, Robinson JT, Mesirov JP. 2013. Integrative Genomics Viewer (IGV):
1503 high-performance genomics data visualization and exploration. *Brief. Bioinform.*
1504 14:178–192.

1505 Valencia-Montoya WA, Pierce NE, Bellono NW. 2024. Evolution of sensory receptors.
1506 *Annu. Rev. Cell Dev. Biol.* 40:353–379.

1507 Wallbank BE, Wheatley GA. 1979. Some responses of cabbage root fly (Delia
1508 brassicae) to allyl isothiocyanate and other volatile constituents of crucifers. *Ann.*
1509 *Appl. Biol.* 91:1–12.

1510 Wang W, Dweck HKM, Talross GJS, Zaidi A, Gendron JM, Carlson JR. 2022. Sugar
1511 sensation and mechanosensation in the egg-laying preference shift of Drosophila
1512 suzukii. *Elife* 11:e81703.

1513 Weiss LA, Dahanukar A, Kwon JY, Banerjee D, Carlson JR. 2011. The molecular and
1514 cellular basis of bitter taste in Drosophila. *Neuron* 69:258–272.

1515 Wheat CW, Vogel H, Wittstock U, Braby MF, Underwood D, Mitchell-Olds T. 2007. The
1516 genetic basis of a plant insect coevolutionary key innovation. *Proceedings of the*
1517 *National Academy of Sciences* 104:20427–20431.

1518 Whiteman NK, Gloss AD, Sackton TB, Groen SC, Humphrey PT, Lapoint RT, Sønderby
1519 IE, Halkier BA, Kocks C, Ausubel FM, et al. 2012. Genes involved in the evolution
1520 of herbivory by a leaf-mining, drosophilid fly. *Genome Biol. Evol.* 4:900–916.

1521 Whiteman NK, Groen SC, Chevasco D, Bear A, Beckwith N, Gregory TR, Denoux C,
1522 Mammarella N, Ausubel FM, Pierce NE. 2011. Mining the plant-herbivore interface
1523 with a leafmining Drosophila of Arabidopsis. *Mol. Ecol.* 20:995–1014.

1524 Wittstock U, Agerbirk N, Stauber EJ, Olsen CE, Hippler M, Mitchell-Olds T, Gershenzon

J, Vogel H. 2004. Successful herbivore attack due to metabolic diversion of a plant chemical defense. *Proc. Natl. Acad. Sci. U. S. A.* 101:4859–4864.

Yang J, Guo H, Jiang N-J, Tang R, Li G-C, Huang L-Q, van Loon JJA, Wang C-Z. 2021. Identification of a gustatory receptor tuned to sinigrin in the cabbage butterfly Pieris rapae. *PLoS Genet.* 17:e1009527.

Yapici N, Cohn R, Schusterreiter C, Ruta V, Vosshall LB, Yapici N, Cohn R, Schusterreiter C, Ruta V, Vosshall LB. 2016. Taste Circuit that Regulates Ingestion by Integrating Food and Hunger Signals Article A Taste Circuit that Regulates Ingestion by Integrating Food and Hunger Signals. *Cell* 165:715–729.

Zhao J, Lin King JV, Paulsen CE, Cheng Y, Julius D. 2020. Irritant-evoked activation and calcium modulation of the TRPA1 receptor. *Nature* 585:141–145.

Zhong L, Bellemer A, Yan H, Honjo K, Robertson J, Hwang RY, Pitt GS, Tracey WD. 2012. Thermosensory and Nonthermosensory Isoforms of Drosophila melanogaster TRPA1 Reveal Heat-Sensor Domains of a ThermoTRP Channel. *Cell Rep.* 1:43–55.